Received: 25 May 2023 | Revised: 21 December 2023 | Accepted: 1 January 2024

DOI: 10.1002/eqe.4083

RESEARCH ARTICLE

WILEY

Collapse hybrid simulation for testing steel building columns subject to boundary condition changes

Konstantinos Skalomenos[1,2] | **Masahiro Kurata**[2]

[1]Department of Civil Engineering, University of Birmingham, Birmingham, UK

[2]Disaster Prevention Research Institute, Kyoto University, Kyoto, Japan

Correspondence
Konstantinos Skalomenos, Department of Civil Engineering, University of Birmingham, Edgbaston, B15 2TT, Birmingham, UK.
Email: k.skalomenos@bham.ac.uk

Funding information
International New Exploratory Research, Grant/Award Number: 2019H-04 / 3604835687; Disaster Prevention Research Institute

Abstract

This paper develops a hybrid simulation to experimentally evaluate the ultimate behavior of steel columns subject to boundary condition changes and bending moment redistribution due to the progressive seismic collapse of building structures. The proposed experimental method combines sub-structuring test techniques and refined finite element (FE) analysis methods in a hybrid scheme. The inelastic behavior of steel moment-resisting-frames (MRF) is computationally simulated while ground-floor columns are physically tested online with the FE frame analysis. Boundary conditions at the interface node between the column test and the frame analysis are reproduced with the aid of three actuators that impose axial loads and bending deformations to the column test. Two square tubular steel columns are tested as part of a five-storey five-bay steel MRF designed to employ two different heights of the ground floor (i.e., 4.6 and 5.1 m, respectively). The hybrid simulation revealed that individual failures of the peripherical frame members significantly alter the distribution of the bending moment along the height of the column test, thus changing the boundary conditions at its top end. The imposed moment distribution was further influenced by local buckling initiated at the base of the column test and ground-floor beams and could cause the top end of the upper-storey columns of the frame to buckle. In the MRF with 4.6 m-height ground-floor, this resulted in a global collapse mechanism that involved the ground floor and the second storey. In the MRF with 5.1 m-height ground-floor, a weak-storey collapse mechanism was formed within the ground floor. Compared to a corresponding isolated column tested as cantilever using conventional methods, the columns tested with the proposed hybrid simulation exhibited a more favorable inelastic behavior primarily due to the more realistic loads and changes of boundary conditions which are ignored in conventional test methods.

KEYWORDS
bending moment redistribution, boundary conditions, collapse, FE model update, hybrid simulation, MRF, steel tubular columns

1 | INTRODUCTION

Structural members are usually tested alone, isolated from the remaining structural system, thus ignoring member–system interaction effects. Studies have indicated that structural members tested as isolated components may exhibit a different performance (inferior or superior) than that of the corresponding members tested within a structural system.[1]

In experimental earthquake and structural engineering, current conventional test methods for isolated structural members consider ideal boundary conditions for member ends for simplicity. These are either fixed-fixed boundary conditions implying that the inflection point (i.e., zero-bending moment location) is located at the mid-length of the member, or fixed-pinned boundary conditions adopting the cantilever end scheme. Therefore, the location of the inflection point is constant throughout the loading. However, in full-scale tests of steel building columns to collapse it has been seen that the seismic performance of steel columns is affected by the boundary conditions of the frame because of the flexibility of the beam-to-column connections intersecting the column.[2–5] Moreover, the internal force redistribution caused by the earlier yielding and local buckling evolution of beams due to the strong-column/weak-beam concept, further affects the boundary conditions at column ends. Such effects gradually become more severe at high inelastic levels of the structural response (near collapse) and can significantly alter loads and boundary conditions in columns.

The necessity for the advancement of structural testing in efficiency has introduced an innovative experimental method, called as "hybrid simulation" or "hybrid testing." The purpose of the method is to take the advantages of experimental and numerical simulations by interactively combining computer simulations with physical test, thus allowing for more realistic definition of the loading and boundary conditions. The method has a history of 50 years[6,7] and is becoming a common test procedure in the field of earthquake and structural engineering.[8,9] Thanks to technology modernization, hybrid simulation is now conducted using better algorithms and advanced hybrid methodologies, such as, substructuring techniques,[9–11] distributed test-analysis domains,[12,13] real-time testing,[14,15] model updating,[16,17] and nonlinear finite element methods.[18–20]

Hybrid simulation divides the entire structural system into substructures, where the part of interest is physically tested (experimental substructure) in parallel with the rest of the structure which is analytically simulated (analytical substructure). In most hybrid simulations the experimental substructures are structural subparts that expected to experience significant inelastic deformations, while the analytical substructure consists of components that expected to remain elastic or almost elastic.[13,15,19] This is because there is much more confidence in the ability of the models to capture a simplified response than a complex inelastic response. Another limitation is associated with the boundary conditions between the experimental and analytical substructure. First studies suggested substructuring structures at zero-moment locations assuming points of inflection represented by pins, thus eliminating control of the rotational degree-of-freedom (DOF) at the interface nodes between test and analytical substructures. This substructuring technique provides reasonable results when a structure experiences moderate yielding, but for collapse assessment, significantly different results have been observed including a change in the collapse mechanism of the structure.[10]

Over the last decade, improved algorithms, advanced test setups, or boundary overlapping techniques have been introduced to provide more accurate results through collapse, with the most recent example the use of multiaxial loading and boundary condition connectors to impose the required DOFs in the test substructure. All previous substructuring techniques have been successful for testing large structural subassemblages[21–23] indicating that hybrid simulation can also be successful for smaller parts of the structures, such as beam and column members, if adequate control of boundary DOFs is ensured at the interface nodes. However, the use of hybrid simulation for isolated members imposes a new challenge, especially when collapse is concerned. Larger part of the structural system should be solved in the analytical domain requiring a higher level of modeling sophistication. This can be possible nowadays thanks to the computational power of several finite element analysis software[24] that can be used in hybrid simulations. The study of Skalomenos et al.[18] demonstrated feasibility of hybrid simulation for testing gusset plate brace connections until fracture by computationally solving the complex cyclic nonlinear behavior of steel tubular braces.[25] Thus, by further expanding refined FE modeling in hybrid simulations to account for larger part of the structure it can turn hybrid test setups into more resource-efficient test setups to target individual structural components.

This paper develops a substructure-based hybrid simulation to investigate the behavior of ground-floor columns of steel building framed structures to collapse. The test method explicitly takes into consideration the change of boundary DOFs at the column ends caused by the movement of the inflection point along the column length as global collapse of the frame is progressed under lateral seismic loads. The test method synchronizes three actuators to control loads and DOFs at the interface node of the column test, while in parallel utilizes sophisticated finite element methods for the analysis of the entire remaining frame structure. The proposed hybrid simulation adopts the nonlinear static

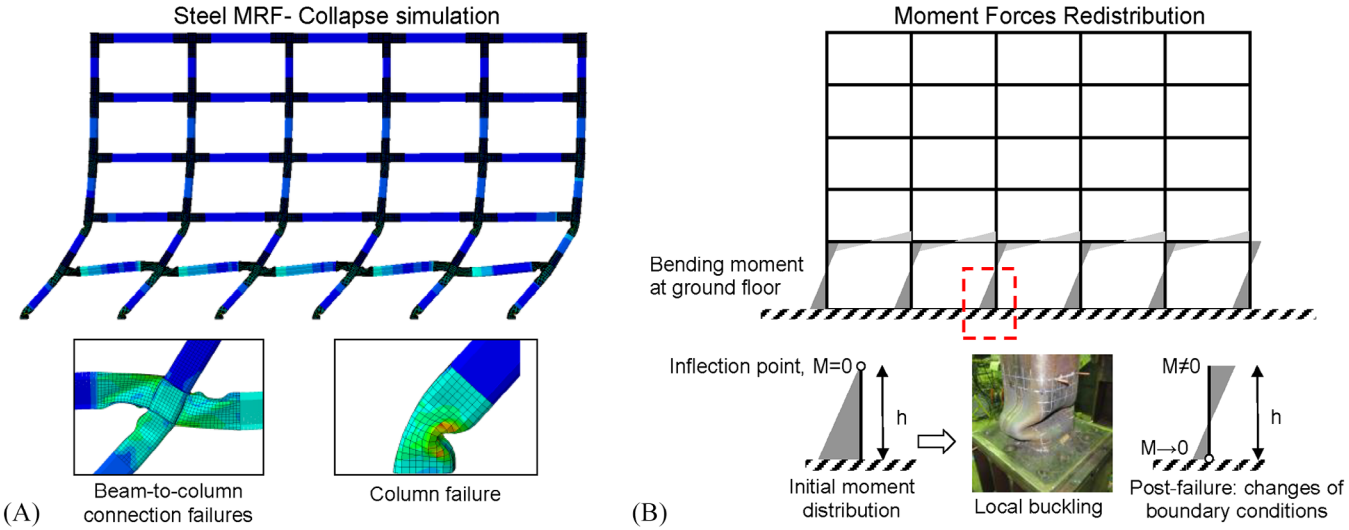

FIGURE 1 (A) Collapse simulation of a steel MRF: deformation of panel zone, and local buckling failures in beams and columns[6]; (B) moment redistribution in columns of ground floor in post-yielding phase of the structural response.

(adaptive pushover) analysis to examine the inelastic seismic force–deformation response of the steel frame to collapse. By identifying the global deformation mechanism of the steel frame, the proposed hybrid simulation successfully alters the moment distribution along the length of the tested column and leads in a more realistic and accurate assessment compared to steel columns tested alone using conventional testing methods.

2 | PROBLEM STATEMENT

2.1 | Overview and novelty of the proposed collapse hybrid simulation

The experimental assessment of the ultimate behavior of steel MRF columns has been a main research topic for many years in the field.[2–5,26–28] This is primarily done by treating the column as an isolated member with a given length and pre-defined boundary conditions. However, at system level, changes that might be caused to column boundary conditions because of the inelastic behavior of the frame may affect column performance. Note that changes to the boundary conditions of a column are usually caused by the progress and sequence of local failures either in the column itself (e.g., yielding, local buckling) or in members of the rest of the structure, such as columns of upper storeys, beams, panel zones, and beam-to-column connections of the MRF (Figure 1A). More specifically, the bending moment at the loading point of a cantilever column test which initially is assumed to be zero (location of the inflection point), shall increase or decrease during the inelastic response of the MRF followed by changes in rotational DOFs at the free end of the tested column (Figure 1B). This alteration of the moment distribution along the column length is strongly dependent on the changes of boundary conditions. To account for these effects when testing steel columns alone, this paper adopts the concept of substructure-based hybrid simulation and develops a novel hybrid test set-up for ground-floor steel columns capable of updating the boundary conditions of the column test through collapse frame simulations.

The proposed hybrid simulation combines refined finite element (FE) simulations executed in ABAQUS[24] with MATLAB optimization algorithms.[29] Its novel points are as follows:

a. It uses "active" advanced numerical methods for structural members and materials instead of "passive" concentrated plasticity models with fixed material responses (e.g., Wang et al.[13] and Del Caprio Ramos et al.[21]). Complex nonlinearities, such as panel zone shear deformations, connection flexibility, local buckling of steel beams and columns, strength, and stiffness deterioration effects, etc., are automatically captured through the refined FE modeling (e.g., shell elements) adopted at critical locations of the structure.
b. It uses fishbone MRF modeling instead of entire frame models for computational efficiency (advanced full-scale FE models are relatively heavy models), as well as novel overlapping boundary substructuring techniques to avoid complex

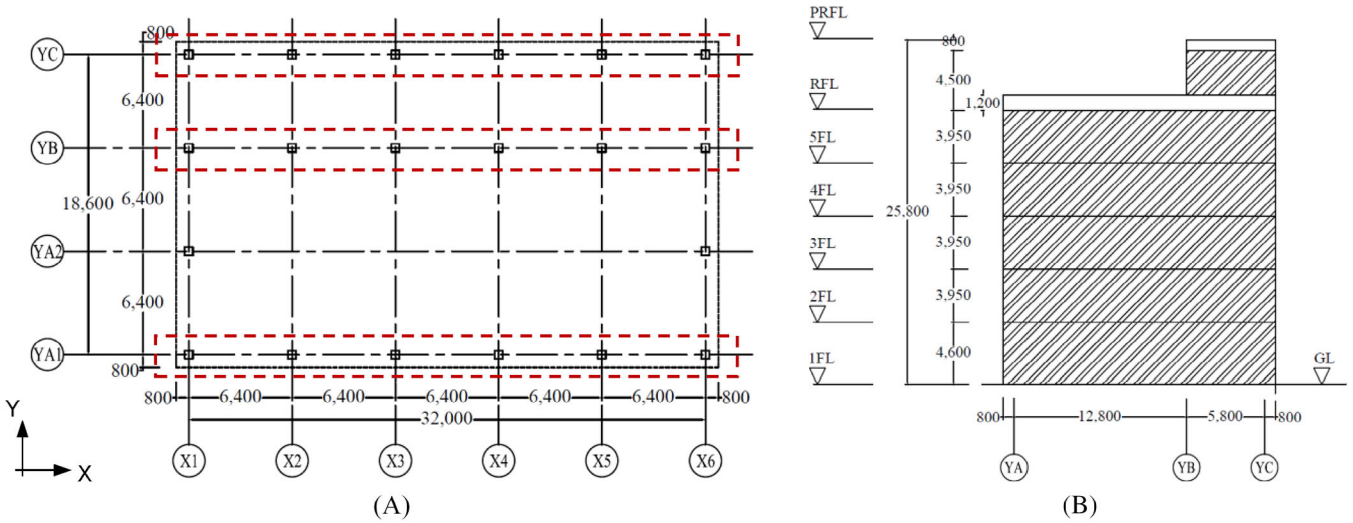

FIGURE 2 (A) Plan view of the building; and (B) side view of the building.

TABLE 1 Column and beam cross-sections, and steel materials.

Floor	Columns	Beam ends	Beam middle	Columns	Beam ends	Beam middle
5	500 × 22	H-600 × 250 × 12 × 19	H-600 × 250 × 12 × 19	BCP325	SN490B	SN490A
4	500 × 22	H-600 × 250 × 12 × 19	H-600 × 250 × 12 × 19	BCP325	SN490B	SN490A
3	500 × 22	H-600 × 250 × 12 × 19	H-600 × 250 × 12 × 19	BCP325	SN490B	SN490A
2	500 × 22	H-600 × 250 × 12 × 22	H-600 × 250 × 12 × 19	BCP325	SN490B	SN490A
1	500 × 22	H-600 × 250 × 12 × 22	H-600 × 250 × 12 × 19	BCP325	SN490B	SN490A

experimental setups. Three actuators that control axial loads, storey drift, and the alteration of the bending moment distribution along the column length are used to reproduce the real boundary conditions between the fishbone MRF simulations and the column test.

c. Non-iterative prediction algorithms are integrated to update all boundary conditions of the fishbone model for accurate frame collapse simulations and implement the test information (non-linear force/stiffness relationship) into the finite element analysis procedure (test informative FE model updating techniques).
d. At this phase it utilizes the common static pushover analysis as a more generalized method for collapse capacity clarification of structures. It can easily utilize the novel cyclic pushover analysis[30] to account for damage accumulation.
e. It utilizes a force-based pushover analysis before and after the post-peak strength point to successfully simulate the collapse mechanism of the structure. It implements a novel optimization procedure at each step to overcome convergence errors in the descending branch of the inelastic response (where traditional force-based pushover analysis cannot proceed) without using computationally demanding stabilization algorithms (e.g., explicit dynamic) or arc-length methods that may become uncontrollable or give erroneous results under certain circumstances.[31]

2.2 | Building structure example

The structure considered in this study is a steel MRF of a prototype five-storey five-bay steel office building designed based on the Japanese seismic design code.[32] It has a rectangular floor plan with aspect ratio equal to 1.70. The longitudinal dimension L_X has length 32.0 m and five bays, while the transverse dimension L_Y has length 18.6 m and three bays. In Figure 2A, the structural system of a typical floor plan is presented while in Figure 2B the elevation of the building is shown. The total building's height is 20.5 m. The structural system illustrated in Figure 2A consists of three planar MRFs along the x-axis and two planar MRFs along the y-axis. The building has square tubular column sections and H beam sections. The cross-section of the columns and beams is given in Table 1. Grade of steels BCP325 and SN490B were adopted for columns and beams, respectively (yielding stress equal to 325 MPa and ultimate strength equal to 490 MPa).[33]

TABLE 2 Seismic demand and seismic capacity.

Floor	Floor weights W_i (kN)	Distribution A_i	Drift requirement forces Q_i (kN)	Design basis forces Q_{un} (kN)	Floor strength Q_u (kN)	Over-strength factor Q_u/Q_{un}	Modal analysis
5	6600	1.743	2662	3328	6844	2.06	4.70
4	5523	1.459	3841	4801	9874	2.06	4.17
3	5523	1.275	4753	5953	12,243	2.06	3.33
2	5538	1.128	5463	6829	14,044	2.06	2.22
1	5567	1.000	5974	7446	15,313	2.06	1.00

The ultimate strength design of the building was achieved through a characteristic factor $D_s = 0.25$ (i.e., behavior factor $q = 4.0$), while the allowable strength and drift limitation requirement of 1/200 was satisfied for a base shear coefficient $C_0 = 0.20$. Table 2 provides the weight of each floor, the A_i load distribution, the seismic forces that correspond to the design basis event, and drift limitation requirement, respectively, the total story strength determined by the cross-sections, and the normalized first mode. The period of the building is 0.94 s along the *x*-axis and 0.90 s along the *y*-axis.

The A_i force distribution is described by the following relation:

$$A_i = 1 + \left(\frac{1}{\sqrt{a_i}} - a_i \right) \frac{2T}{1 + 3T} \tag{1}$$

where a_i and T are obtained by:

$$a_i = \frac{\sum W_i}{W} \tag{2}$$

and:

$$T = H \cdot (0.02 + 0.01 \cdot \alpha) \tag{3}$$

In Equation (2), W is the total weight of the structure, ΣW_i is the summation of the weights of all storeys above of the storey i, H the total building height, and α equals 1.0 for steel buildings (along the height). The structural period T is 0.62 s.

3 | DESIGN OF THE HYBRID SIMULATION

3.1 | Concept and substructuring techniques

The concept of the test method is illustrated in Figure 3A. One plane steel MRF of the three along the *X* direction shown in Figure 2 is considered. The steel MRF is divided into two parts: (a) the numerical; and (b) the experimental substructure. The experimental substructure is the column at the ground floor of the building, while the rest of the structure is the numerical substructure. The numerical model is created with the aid of the FE analysis software ABAQUS,[24] capable of simulating the non-linear behavior of frame components with emphasis to panel zone shear deformation and local buckling related failures in beams and columns.[33] Fracture is not simulated in the present study. Details of the frame FE model are given in Section 5. The test of the column specimen is carried out in order to acquire accurate information about the restoring force and stiffness of the ground-floor column. Thus, the restoring forces are experimentally measured and applied to the numerical substructure to reproduce the actual restraint and strength of the ground-floor column.

The hybrid test is conducted in many steps *i*. In the proposed hybrid simulation, the response of the framed column of interest (i.e., ground-floor column) is simulated by using an elastic beam-column element plus a non-linear rotational spring with constant $K_{\theta,i}$ located at the base of the column. The elastic element is to account for the linear response of the column while the nonlinear element is to account for the flexibility of the column base connection and the plastic deformation of the column itself (i.e., plastic hinge), as shown in Figure 3B. The nonlinear spring properties are defined by the substructure column test. Loads and rotations are imposed to the substructure column test by means of three actuators as it is explained later. The input of these quantities is obtained from the frame FE analysis which is performed online with the experiment. At each loading step *i*, the restoring bending moment at the base ($M_{b,i}$) and top ($M_{t,i}$) of the

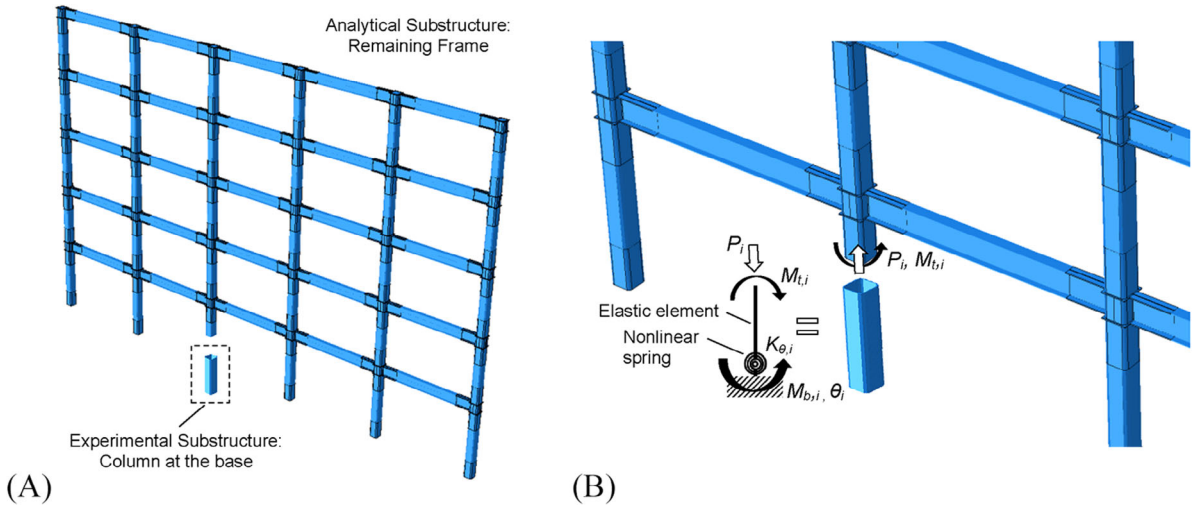

FIGURE 3 (A) Sub-structuring concept; (B) on-line update of the FE model utilizing experimental quantities.

substructure column test is experimentally measured and is used in the following step i+1 together with the corresponding experimental θ_i at the base of the column to predict the nonlinear spring constant $K_{\theta,i+1}$ of the numerical model. Note that for the prediction of $K_{\theta,i+1}$, the elastic rotation of the column needs to be subtracted from the measured θ_i. For the calculation of the elastic rotation as part of the experimental measurement, the initial stiffness of the framed column is used. This can be determined by performing an elastic frame FE analysis. The above substructuring technique adopts to some extent overlapping domain[21] between the experimental and analytical substructures to avoid control of three boundary conditions at the substruction cross-section,[22] thus simplifying the hybrid test set-up. This is essential in the present study as in addition to the $M_{b,i}$ induced at the bottom of the substructure column test, $M_{t,i}$ is also applied to the top end of the same column (Figure 3A).

With known $K_{\theta,i+1}$, the next analysis step i+1 is performed with the updated model. The structure is successfully driven by the pushover loads to the new $M_{b,i+1}$ and θ_{i+1} predictions, as explained in the next section (Section 3.3). To eliminate or minimize the cumulation of any error between "predicted" analytical and "actual" experimental values, the differences between the numerical and experimental bending moment of the previous analysis step i are imposed as pseudo external bending moment at the i+1 analysis step to compensate the over-estimation or under-estimation of the actual column restraint.[18] A restart analysis procedure featured by ABAQUS[24] is repeatedly used to accommodate the restored information of the experiment into the FE model at each step operating a MATLAB[29] main program. The rationality of the proposed hybrid simulation is proved in a later section (Section 7.2) where experimental column rotations are found to be very close to those obtained from the numerical model. In the future, validations of the proposed procedure through comparison with tests carried out on full frames can further explore the rationality of the proposed method.

3.2 | Restart capability of ABAQUS

ABAQUS[24] offers the capability of restart analysis, which enables the user to stop the analysis at a desired time point and restart at the same or another time point the analysis of an updated version of the model already analyzed. Each increment of the proposed hybrid simulation includes a restart analysis, in which the model definitions and all information of the current analysis state is written in a set of restart files. The ABAQUS input file is properly updated based on the specified loading definitions in conjunction with the response of the structure calculated so far, and finally the updated input file along with the restart files written at the current increment are read by the restart ABAQUS analysis calculating thus the structural response at the next increment.

3.3 | Prediction quantities

To assure a reasonable accuracy of the hybrid test, a sufficiently large number of loading increments are needed to minimize the error imposed by the difference between the actual column restraint and that of analysis. Iterative restart analysis

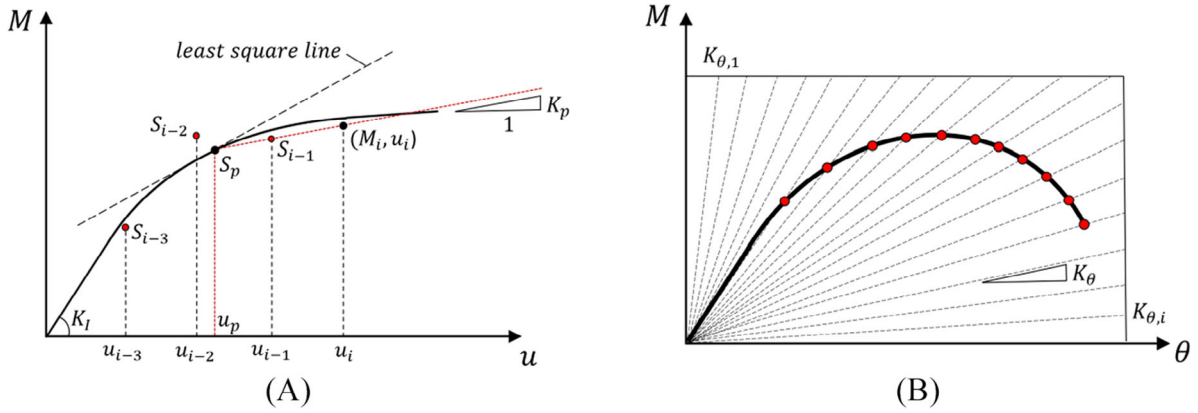

FIGURE 4 (A) Procedure of moment M_i prediction using three sample test data[9]; (B) a schematic approximation of the predefined values concept for $K_{\theta,i}$ as defined in the initial input of FE model (Field variables[27]).

to achieve convergence within the same loading increment could minimize the introduced error. However, iterative restart analysis may not be acceptable in on-line hybrid tests that involve physical testing because it is impractical to return the test structure to a previous position once has been loaded in elastically. The iteration can be avoided by integrating a force/stiffness prediction algorithm along with a compensation of the imbalance restoring forces (pseudo external forces). The pseudo external force is the result of the difference between the predicted and actual column restraint as discussed in the previous section.

The approach adopted in this study gives the option of updating incremental quantities of the frame FE analysis at each loading step on the basis of the test information. Figure 4 illustrates an example of the procedure for predicting the moment M_i using at least three sample data from the test. The adopted prediction algorithm[9] uses the least square method to determine the slope and intercept values of a linear function, $f(u)$, that represents the linear fit of n sets of previous sample data $S_{i-j}(u_{i-j}, M_{i-j})$, where u_{i-j} and M_{i-j} are the roof displacement and base moment of the $i-j$ step, where $j = n, \ldots, 3, 2, 1$. Then, using S_{i-1}, a new set of data (u_p, M_p) is determined on the linear function $f(u)$ as shown in Figure 4A. The new data are taken as

$$u_p = \frac{\sum_{i=j-n}^{j-1} u_i}{n} \tag{4}$$

$$M_p = f\left(u_p\right) = Slope \times u_p + Intercept \tag{5}$$

The following step is to predict the force M_i at u_i using a linear extrapolation based on the two sets of data, (u_p, M_p) and (u_{i-1}, M_{i-1}),

$$M_i = (u_i - u_p) \times K_p + M_p \tag{6}$$

where K_p is taken as

$$K_p = \frac{(M_{i-1} - M_p)}{(u_{i-1} - u_p)} \tag{7}$$

An example is given in Figure 4A. S_1, S_2, and S_3 are the data of the previous three steps. The linear function $f(u)$ is defined using the least square method based on these three data. The point S_p is defined by employing Equations (4) and (5). The predicted moment M_i is calculated based on S_p by employing Equations (6) and (7). The above procedure is repeated to predict the rotation θ_i of the column base (see Figure 3) at every u_i. $K_{\theta,i}$ is then estimated for the following analysis step as

$$K_{\theta,i} = \frac{M_i}{\theta_i} \tag{8}$$

Note that $K_{\theta,i}$ is the constant of a nonlinear spring defined explicitly for a pair of M_i and θ_i. ABAQUS[24] understands $K_{\theta,i}$ as secant stiffness for controlling the nonlinear response of the rotational spring. In the proposed hybrid test method, possible values for $K_{\theta,i}$ are all pre-defined in the first input file of the FE model in ABAQUS[24] through field variables (*DEPENDENCIES = 1). Field variables can be made solution dependent, which allows for introducing additional nonlinearities in the FE analysis during the restart analysis. The magnitude of the field can be prescribed at the specific node of the model using the test results and the prediction algorithm, and ABAQUS restart algorithms will interpolate the values within the predefined range. Figure 4B illustrates a schematic approximation of the concept for the predefined spring constants as this was defined in the first input file of the FE model. At every analysis step i of the hybrid simulation, the bending moment M_i is computed for a given θ_i as instructed by $K_{\theta,i}$. It should be noted that the first steps of the hybrid test were performed by considering a constant value of $K_{\theta,i}$ for the spring at the base of the column in order to generate first a reasonable sample data (three to four values) to process. Then, the prediction algorithm is automatically activated. The initial constant value for $K_{\theta,i}$ is determined by performing a preliminary hybrid test of the column specimen within the elastic range.

3.4 | Pushover analysis: adaptivity and descending branch

Static pushover analysis has been widely used in earthquake engineering and design of buildings, such as in the Capacity Spectrum Method (CSM).[34] Among the advantages of the pushover analysis method are that it is simple, fast, and provides all the capacity aspects of a structure until collapse.[30,35] In an attempt to increase the accuracy of the results of the pushover analysis, adaptive force or displacement patterns are considered during the analysis. Adaptivity is realized in a way that ensures that the force or displacement pattern imposed on the building during the pushover analysis is continually updated depending on the instantaneous dynamic characteristics of the structure and/or a site-specific spectrum. Among the first studies that have introduced procedures to utilize fully adaptive patterns for pushover analysis is.[36]

A comprehensive presentation of the importance and various special traits of the pushover curve can be found in Elnashai[37] and Hall. [38] It is shown that the slope of the descending branch of any pushover curve depends strongly on the level of modeling sophistication, elastic unloading of the storeys not participating in the collapse mechanism, and on the static or dynamic nature of the pushover algorithm. This implies that the use of simplified plastic hinge formulations may not apply for tracing the descending branch accurately.[39]

An advanced modeling through FE methods would be beneficial to accurately capture the descending branch of a pushover curve and finally the collapse mechanism. However, to trace accurately the descending branch in a force-controlled pushover analysis is generally difficult (almost impossible with normal static analysis) since once the maximum capacity is reached the lateral loads cannot increase further. In addition, the use of advanced modeling approaches often generates convergence errors (strain concentration etc.) that terminate the analysis at an early stage. To overcome these problems, the present study introduces a novel and stable mixed force–displacement control algorithm that implements an optimization procedure to mainly perform a force-based pushover analysis before and after the post-peak strength point, thus capturing the collapse mechanism and descending branch of the pushover curve, that is, not accurately captured in displacement-based pushover analysis.

4 | TECHNICAL FEATURES OF THE COLLAPSE HYBRID SIMULATION

4.1 | Static analysis algorithm versus arc-length control

It is noted that if the force distribution is to be updated according to the first or a number of eigenmodes of the structure during the adaptive pushover analysis, none of the analysis types offered by ABAQUS[24] can be used since (in the best case) they preserve the load distribution until the analysis is ended. Two types of nonlinear static analysis procedures can be carried out in ABAQUS[24] in order to perform static pushover analysis of any structural model, which are described below, along with their limitations:

- *Static analysis with force control*. Even in a non-adaptive pushover analysis, it is recognized that this type of ABAQUS analysis cannot be used with force-control to trace the descending branch of the inelastic response, as already mentioned in a previous section. Therefore, neither for an adaptive, nor for a non-adaptive constant load pattern pushover analysis can be used.

- *Static analysis with arc-length control (Riks)*. Assuming that the model is loaded with forces of constant pattern, although this analysis can rarely trace the descending branch of the inelastic structural response, it can trace only a single loading path during the analysis and does not allow the user for control over the force distribution pattern during the pushover analysis. Therefore, for an adaptive load pattern pushover analysis, this type of analysis cannot be used.

Since the static Riks analysis with arc-length control cannot distinguish between loading and unloading directions, if the step of the restart analysis is a static Riks step, there is the possibility that the analysis starts from a point different from the last converged equilibrium point and apply the loading in a direction opposite to the one specified, leading thus the structure to unexpected unloading instead of reloading condition. For the above reasons, in this study the restart analysis is used only with general static analysis. Details about the way in which restart static analysis capability is incorporated in the adaptive pushover analysis implemented in this study are given at a following section.

4.2 | Mixed force–displacement optimization control for the descending branch

In the proposed hybrid simulation, the descending branch of the inelastic response of the structure is traced with mixed force/displacement control developed by Skalomenos and Papazafeiropoulos.[31] Displacement control is applied by directly specifying the desired displacement at the top of the structure. Force control is applied indirectly through an optimization procedure which ensures that the force pattern is maintained or appropriately updated along the height of the structure throughout the pushover analysis. With repeated use of the restart capability, ABAQUS[24] can be consistent with the quasi-static structural loading response.

In each increment of the pushover analysis procedure, that is, proposed in the proposed hybrid simulation, a static analysis is performed in which both forces and roof displacement are imposed at the structure. The forces and displacement are imposed in a controlled manner that ensures the linear dependence between the actual force distribution imposed at the structure, $\{\tilde{F}_i\}$, and the desired force distribution, that is, based on its fundamental eigenmode, $\{\bar{F}_i\}$, that is, that the following relation is satisfied at all stories of the structure:

$$\tilde{F}_i\ (j) = \lambda_i\, \bar{F}_i\,(j)\,,\ j\ =\ 1,\dots,5 \tag{9}$$

Since the way of computation of the load proportionality factor λ_i at the i^{th} increment of pushover analysis is not straightforward, it is indirectly calculated through the implementation of an optimization procedure. The optimization problem, that is, considered at each increment of the pushover analysis is to find the optimum load proportionality factor λ_i that minimizes the variance of the vector defined by the division of $\{\tilde{F}_i\}$ by $\{\bar{F}_i\}$ in an element-wise manner:

$$R_i\ (j) = \frac{\tilde{F}_i\,(j)}{\bar{F}_i\,(j)}\,,\ j\ =\ 1,\dots,5 \tag{10}$$

If $\mathrm{v}ar(R_i) =\ 0$ this means that all the elements of the vector R_i are equal with each other, and equal to λ_i, since it is always $\mathrm{v}ar(R_i) \geq 0$ by definition. The design variable of the optimization problem is the scalar λ_i and the objective function to be minimized is equal to $F_i^{obj} = \mathrm{v}ar(R_i)$.

The original inequality-constrained minimization problem, that is, solved in each increment of the mixed force–displacement controlled pushover analysis is described by:

$$\min_{\lambda_i}\{\mathrm{v}ar\,(R_i)\}\ \text{subjectto}\ :\ \mathrm{g}\ (\lambda_i) = \begin{bmatrix}\lambda_i - \lambda_{ub,i}\\ \lambda_{lb,i} - \lambda_i\end{bmatrix}\ \leq \begin{bmatrix}0\\0\end{bmatrix} \tag{11}$$

where $\lambda_{ub,i}$ and $\lambda_{lb,i}$ the upper and lower bounds of λ_i for the optimization procedure, respectively. The optimization algorithm considered in this study for the solution of the optimization problem is the Interior Point Algorithm (IPA). This method is described in Waltz et al.[39] According to this algorithm, Equation (12) is solved as a sequence of the following approximate equality-constrained minimization problems for $\mu > 0$:

$$\min_{\lambda_i,s}\ \left\{F_{i,\mu}^{obj}\,(\lambda_i,s)\right\} = \min_{\lambda_i,s}\ \left\{F_i^{obj}\,(\lambda_i)\right\} - \mu\sum_j \ln\left(s_j\right)\ \text{subjectto}\ :\ g\,(\lambda_i) + s\ =\ 0 \tag{12}$$

where $F_i^{obj} = var(R_i)$. There is one slack variable ($s_j \geq 0$) for each inequality j. The number of slack variables of the optimization problem is 2. As μ decreases to zero, the minimum of $\{F_{i,\mu}^{obj}(\lambda_i, s)\}$ and the minimum of $\{F_i^{obj}(\lambda_i)\}$ should coincide.

4.3 | Frequency analysis for adaptivity

As discussed above, the proposed hybrid test method uses adaptive pushover analysis to examine the static force–deformation response of building structure to collapse. In each increment of the pushover analysis, the load pattern, that is, applied to the structure has the shape of the first eigenmode of the structure. For this purpose, a frequency analysis is performed in ABAQUS[24] to obtain the fundamental eigenmode and is repeated at every restart step to reflect the non-linearities into the stiffness matrix. To solve the eigenproblem, a shifted block Lanczos algorithm is used, similar to that developed and described in detail by Grimes et al.[40]

4.4 | Analysis control algorithm

The novel adaptive pushover analysis proposed in this study can be carried out by any software that provides for the following essential characteristics:

- A finite element solver to trace the nonlinear response of the structure.
- A constitutive material model which utilizes plasticity, degradation, and damage to update the stiffness of the structure.
- A frequency analysis capability to update the load pattern based on the first eigenmode of the structure (necessary for any adaptive pushover analysis).
- A restart analysis capability to update the restoring forces and displacement profiles imposed on the structure (necessary for the hybrid test).

ABAQUS[24] provides for all of the above capabilities whereas MATLAB[29] is adopted in this study as a suitable tool for post-processing the analysis results. More specifically, the application *Abaqus2Matlab*,[41] which coordinates *Matlab* and *Abaqus* in a loop provides for the updating of the model information for the restart analysis scanning all desired values of roof drifts, and within the optimization analysis associated with the mixed force–displacement control static analysis at each increment of the pushover analysis. The overall computational procedure of the adaptive pushover method for the proposed hybrid test method is presented in Table 3. The objective function, that is, used for the optimization procedure in line 24 of Table 3 is presented in Table 4. Note that although displacement is applied in the top of the structure during analysis, the proposed computational procedure is a force-based pushover analysis until global collapse thanks to the proposed optimization control algorithm.

4.5 | Main program for hybrid simulation control

The flow chart of the main control program developed for the proposed hybrid simulation is described in Figure 5. Two subroutines supervise the analytical and experimental substructures, respectively, and send feedback information to the main control program. The ‘‘FE analysis control subroutine” shown on the left-hand side refers to the numerical substructure, that is, steel frame, while the ‘‘test control subroutine” shown on the right-hand side refers to the experimental substructure, that is, the ground-floor column (Figure 3).

The primary tasks of the main control program are: (a) to send the target roof displacement and update the numerical substructure based on the measured restoring force and stiffness; (b) to receive the analysis information; and (c) to send the target loading and deformation conditions to the physical test, and (d) to obtain the experimental data in order to predict the rotational stiffness and calculate the pseudo external moment. The major functions of the analysis control subroutine are: (a) to create the input files for the FE analysis and upgrade the model using the matched rotational stiffness and the pseudo external moment; (b) to perform the adaptive pushover analysis as described in Tables 3 and 4; and (c) to read and process the analysis results, such as axial force, bending moments, and target displacement (i.e., drift) of the column

TABLE 3 Computational procedure of the adaptive pushover method for the proposed hybrid simulation.

Generic adaptive pushover analysis procedure for ABAQUS
01: Begin
02: Input parameters: roof drift history protocol D_h, height of the building h_{str}, initial upper bound $\lambda_{ub,0}$ and initial lower bound $\lambda_{lb,0}$ for the optimization of the load proportionality factor λ_i
03: Perform static analysis to account for gravity loading at the structure
04: Perform frequency analysis of structure. Obtain the initial fundamental eigenmode $\{\varphi_{1,0}\}$ for stiffness equal to K_0
05: Calculate the initial force distribution $\{F_0\} = [M]\{\varphi_{1,0}\}$
06: Normalize $\{F_0\}$ by setting $\{\bar{F}_0\} = \{F_0\}/F_0(1)$, where $F_0(1)$ is the value of the force distribution at the top floor (roof) of the structure.
07: Set the initial load proportionality factor $\lambda_1 = 1$
08: Calculate the force vector $\{\tilde{F}_1\} = \lambda_1 \{\bar{F}_0\}$
09: Perform static analysis to account for gravity loading at the structure
10: Perform force-controlled static analysis of the structure for the force distribution $\{\tilde{F}_1\}$
11: Obtain the floor displacements $\{u_1\}$ due to load distribution $\{\tilde{F}_1\}$
12: Calculate the roof drift $dr_1 = \frac{u_1(1)}{h_{str}}$
13: Save selected variables into txt files for further postprocessing.
14: For i from 1 to the number of values contained in D_h
15: Perform frequency analysis of structure in the state it was at the $(i-1)^{th}$ increment, in which its stiffness matrix is equal to K_i. Obtain the fundamental eigenmode $\{\varphi_{1,i}\{\}\}$
16: Find the force distribution $\{F_i\} = [M]\{\varphi_{1,i}\{\}\}$
17: Normalize $\{F_i\}$ by setting $\{\bar{F}_i\} = \{F_i\}/F_i(1)$, where $F_i(1)$ is the value of the force distribution at the top floor (roof) of the structure at the i^{th} increment of pushover analysis
18: Determine the upper and lower bounds of λ_i for the optimization procedure
19: If $\lambda_{i-1} > 0$
20: Upper bound $\lambda_{ub,i} = 2\lambda_{i-1}$
21: Lower bound $\lambda_{lb,i} = \frac{\lambda_{i-1}}{2}$
22: end
23: Calculate the current roof drift for which λ_i is searched, $u_i(1) = h_{str}\, dr_i$.
24: Find λ_i from an optimization procedure, with initial guess λ_{i-1}, bounds $\lambda_{ub,i}$, $\lambda_{lb,i}$, and objective function $F_i^{obj}(\lambda_i)$, so that the roof displacement of the structure is equal to $u_i(1)$, when loaded by a force distribution equal to $\{\tilde{F}_i\} = \lambda_i \{\bar{F}_i\}$
25: Save selected variables into txt files for further postprocessing.
26: end
27: Stop

subassembly. The test control subroutine supervises the test structure by imposing signals to the actuators and by collecting the experimental data. The measured restoring force of the test is applied in the following analytical step. Figure 5 shows the flowchart of the relations between the main program and the subroutines. For the main control program to start, a zero restoring force is imposed to the column base at the initial step.

5 | ANALYTICAL SUBSTRUCTURE

5.1 | Frame modeling

The plane frame shown in Figure 3A is modeled in ABAQUS[24] using the fishbone sub-structuring technique to reduce the computational time.[42] Figure 6 presents the overall view and modeling details of the fishbone model. The frame model

TABLE 4 Description of the objective function.

Objective function $F_i^{obj}(\lambda_i)$
01: Begin
02: Input parameters: load proportionality factor λ_i
03: Parameters updated outside the objective function: normalized force distribution $\{\bar{F}_i\}$,
roof displacement of the structure $u_i(1)$,
04: Calculate the force distribution $\{\tilde{F}_i\} = \lambda_i \{\bar{F}_i\}$
05: Perform static analysis of the structure in which the force distribution $\{\tilde{F}_i\}$ is applied at all stories except for the
roof (i.e., $\tilde{F}_i(1)$ is ignored). Displacement equal to $u_i(1)$ is imposed at the roof.
06: Obtain the reaction force RF_i at the roof of the structure from the static analysis
07: Set $\tilde{F}_i\,(1) = RF_i$
08: Calculate the vector R_i, where $R_i\,(j) = \frac{\tilde{F}_i(j)}{\bar{F}_i(j)}$, $j = 1, \ldots, 5$, where j is the number of storeys of the structure
09: Calculate the variance of the vector R_i, $\mathrm{var}(R_i)$. Return this as the output of the objective function F_i^{obj}
10: Stop

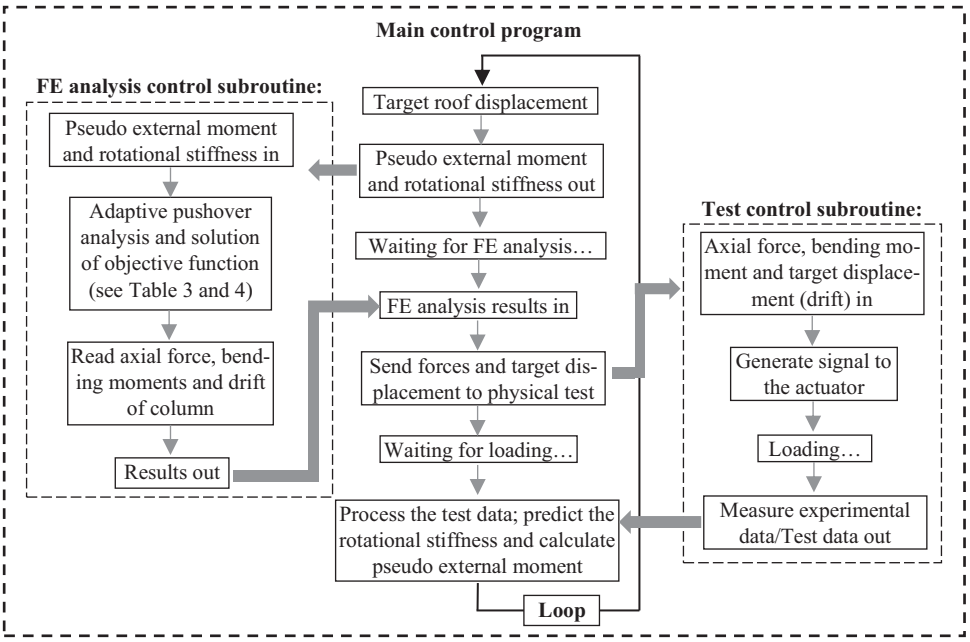

FIGURE 5 Main control program used for the hybrid test method.

developed herein is a mixed shell/beam element model that combines powerful nonlinear shell elements with simple beam-column elements and is referred to as the fishbone model of the structure. These beam-column joints are connected in a height wise fashion with columns.

Shell elements are used in the critical regions of the building, such as column and beam ends, and panel zones, where cross-sectional instabilities (e.g., local buckling) are expected. More specifically, three dimensional 4-node reduced integration shell elements with hourglass control (S4R) are used. These shell elements account for finite membrane strains and arbitrarily large rotations, and therefore they are suitable for large strain analysis. Moreover, these elements are based on first-order transverse shear flexible theory in which the transverse shear strain is assumed to be constant through the thickness of the shell. The shell elements are used for a length equal to twice the width of column and beam depth, respectively, in order to accurately capture the local buckling initiation and post-local buckling response (plastic hinge zone). It has been observed in previous experiments and detailed finite element analyses that this is an adequate length for the formation of the plastic hinge.[33] The beam-to-column connection is fully restrained by diaphragm plates located at the bottom and top of the panel-zone height and simulates a rigid welded connection. The welding access hole was not considered.

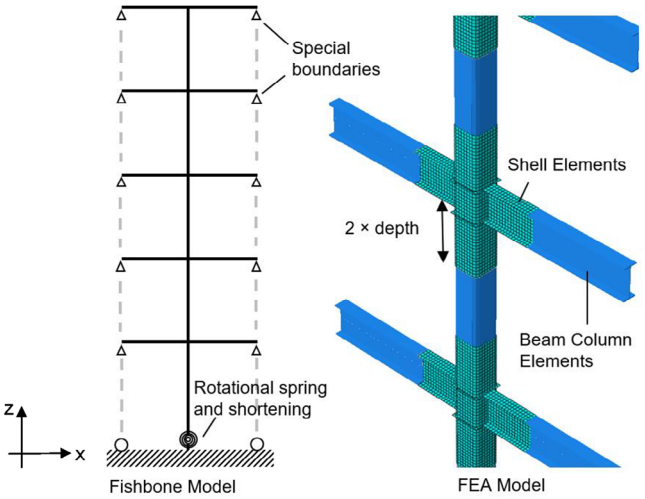

FIGURE 6 Fishbone model in ABAQUS.[24]

Beam-column elements are used for the rest of the length of beams and columns, which is expected to remain mainly in the elastic region. Two-node linear Timoshenko beams in space (B31), which allow for transverse shear deformation are used for the discretization of beam-column elements. It is assumed that the shear behavior of the beam elements used in the model is linear elastic with a fixed modulus and, thus, independent of the response of the beam section to axial stretch and bending. Moreover, the H section of the beam elements is numerically integrated during the analysis, in order to capture the nonlinear material response in the section. The connection between the beam elements of the model and the beam-to-column shell joints is achieved through the imposition of multi-point constraints between the end of the beam or column to be connected to the joint (master node) and the points along the perimeter of the section of the end of the joint (slave nodes). The constraint is imposed by providing dummy rigid beams between the master node and the slave nodes, constraining both the displacement and rotation in a way that corresponds to the presence of a rigid beam between each node pair. The inertia that comes from each floor is modeled by adding mass elements (MASS) at specific points of the beam-to-column joints which is essential for the frequency restart analysis.

Forces and/or displacements are applied at the centers of the beam-column joints to perform a static analysis of the model. Gravity load as well as material and geometric nonlinearities are considered in the static analysis, that is, performed at each step of the adaptive pushover analysis. Regarding the material constitutive model, for sufficiently small strains, steel is modeled as a linear elastic isotropic material with density $\rho = 7850$ kg/m^3, modulus of elasticity $E = 205$ GPa, and Poisson ratio $\nu = 0.3$. For large strains, this constitutive model includes von-Mises yield criterion with kinematic hardening and is suitable to simulate the inelastic behavior of metals under cyclic loading (combined isotropic-kinematic hardening model). A strain hardening slope of 1.0% of the modulus of elasticity was assumed as recommended in EN 1993-1-5.[43] This value has been found to be conservative for some cases but suitable for performing global inelastic seismic analysis in steel framed structures.[44] Using actual material response characteristics as obtained from material coupon tests is expected to lead to more reliable predictions of the structural performance.[33]

5.2 | Update of fishbone boundary conditions and axial loads for collapse simulations

The inelastic behavior of the ground-floor column is simulated through the non-linear moment–rotation spring. At each restart analysis step the spring constant is calculated using the experimental data, as discussed in a previous section. Regarding the boundary conditions of the fishbone model, all six degrees of freedom are fixed at the base of the model, whereas only displacement and rotation along global x and y direction, respectively, are freely permitted for the extreme ends of the beams at each storey, to enhance the diaphragmatic action of the storeys (Figure 6). Out of plane displacements of the beam-column joints (along the global y-axis) are constrained. It should be noted here that a special treatment was set regarding the vertical displacements (global z direction) of the beam ends and the base of the ground-floor column (i.e., region of plastic hinge due to local buckling, as shown in Figure 1B), as shown in Figure 6. For a successful collapse simulation, the vertical displacement of the beam ends of each storey should follow the one of the center of the corresponding beam-to-column joint, whereas the vertical axial shortening of the ground-floor column

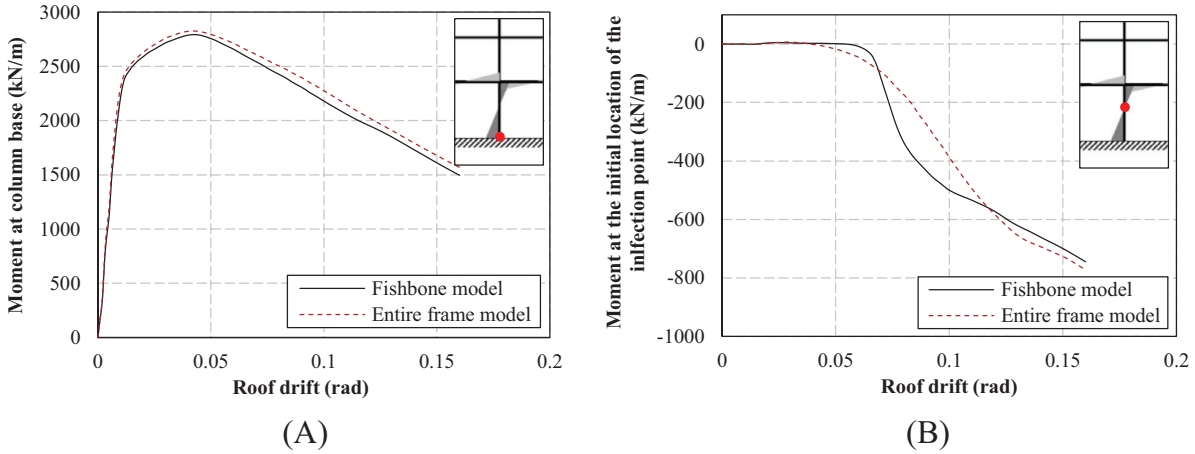

FIGURE 7 Comparison between fishbone and entire frame analysis model: (A) bending moment–roof drift relationship at the base of the ground floor column; (B) moment–roof drift relationship at the initial location of the inflection point.

at the base caused by the evolution of local buckling during the column test should be transferred into the analytical substructure. As a result, a prediction algorithm was set using the procedure introduced in Section 3.3 to predict both the vertical displacement of the beam ends of each storey and the axial shortening of the column base at every step of u_i, thus accurately updating the boundary conditions of the input file of the FE model (i.e., using the command in the restart file: "*Boundary,op = new"). Note that the vertical displacement of beam ends was predicted using computational data of previous analysis steps, while the axial shortening of the column using experimental data. Regarding the axial loads, these are updated using the force equilibrium at every step based on the calculated overturning moment and the location of the examined column (i.e., internal or external column). All the above technical features of the proposed hybrid simulation are possible due to the restart capability of ABAQUS[24] that enables the user to update the model at every loading step.

5.3 | Comparison between fishbone and entire frame model analysis

Figure 7 compares the FE analysis results obtained from the fishbone MRF model with those FE analysis results obtained from the five-storey five-bay MRF model shown in Figure 1A. It should be mentioned here that for the purpose of comparison, instead of placing a rotational spring at the base of the fishbone model as shown in Figure 6, the column at the base of the ground floor was modeled using discretized shell elements, as shown in Figure 1A. The ground floor height in this model has a length of 4.6 m. Figure 7A illustrates the bending moment–roof drift relationship at the base of the ground-floor column, while Figure 7B illustrates the bending moment–roof drift relationship at the initial location of the inflection point of the ground-floor column. One can observe that both analysis models provided similar results, while fishbone model was successful in simulating the same collapse mechanism (ground floor–second storey) with the full MRF model. This was possible due to the continuous update of the fishbone boundaries at the beams ends (vertical displacements) during collapse, as explained in the previous section. As shown in Figure 7B, in both models the bending moment at the initial location of the inflection point remained zero until a roof drift equal to 0.06 radians, and then took negative values until the end of analysis. This indicates that the proposed fishbone modeling technique can produce a similar behavior with the entire full-scale frame model and be a reliable and rational substitute of the original analytical substructure, thus optimizing computational time at no expense of accuracy.

6 | HYBRID TEST SET-UP AND LOADING SYSTEM

6.1 | Loading system and test set-up

Three hydraulic actuators have been considered to ensure physical continuity between the analytical and experimental substructures by controlling axial loads, column drifts, and column boundaries change during the hybrid tests. Figure 8 illustrates the hybrid test set-up. One actuator is placed vertically to impose the axial load (Actuator 1: force control), while the other two actuators are placed horizontally to apply the column rotation (Actuator 2: displacement control) and the

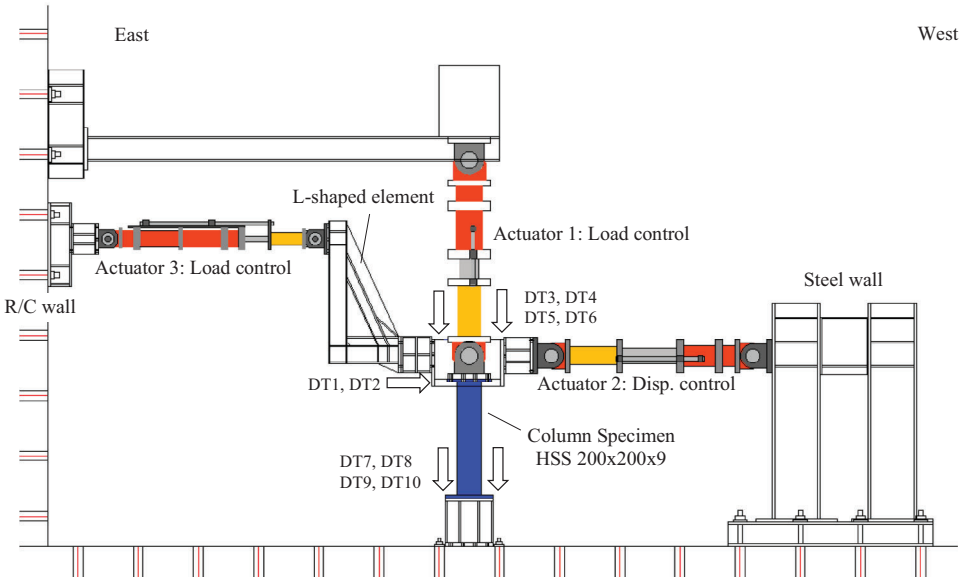

FIGURE 8 Test set-up for the online hybrid test.

TABLE 5 Dimensions of test specimens.

Specimen	Width, d (mm)	Thickness, t (mm)	Carver curvature, r	Height of specimen, h (mm)	Height of ground floor of the building, H_1 (mm) (Figure 2)
SP1	200	9	3.5t	1030	4600
SP2	200	9	3.5t	1420	5100
Isolated column	200	9	3.5t	1030	4600

bending moment at the column top (Actuator 3: load control), respectively. The L-shaped element was designed to be as rigid as possible. Linear strain-gauge type displacement traducers (DT1 to DT10) were used to measure the rotation of the column top and basement as well as lateral story drifts.

6.2 | Test specimens

Table 5 lists details of the test specimens. Two reduced scale column specimens were tested with different length that corresponds to a different height of the ground floor of the frame. The dimensions of the steel section of the column were scaled to 2/5 of the prototype full-scale frame design shown in Figure 2. The first specimen (SP1) had a clear height of 802 mm while its total height measured from the column bottom to the pin end of the vertical actuator was equal to $h_{SP1} = 1030$ mm (see Figure 8). The ground floor of the corresponding full-scale FE model of the SP1 had a height of 4000 mm excluding the beam height (total height of ground floor is 1.16 times the height of each storey above). The second specimen (SP2) had a clear height $h_{SP2} = 1192$ mm while its total height measured from the column bottom to the center of the pin end of vertical actuator was equal to 1420 mm. The ground floor of the corresponding full-scale FE model of the SP2 had a height of 4500 mm excluding the beam height (total height of ground floor is 1.30 times the height of each storey above). The length of each column was selected assuming that the inflection point is located at 0.65–0.75 times the clear height of the ground floor. The column specimens were fabricated by cold formed square hollow structural steel (HSS) sections made of SN490B plate material (assumed equivalent to BCP325). The HSS sections had width $d = 200$ mm, thickness $t = 9$ mm and corner curvature $r = 3.5t$.[32] End plates of dimensions 400 × 400 × 28 and 400 × 400 × 16 were welded through full penetration welds at the bottom and top of the column sections, respectively, to serve as connecting parts to the test set-up (Figure 8). Coupons were also extracted from the flange and corners of the HSS sections to explore the material properties, such as, elastic modulus, yield stress (YS), ultimate stress (US), strain measured at US, and strain at US, as shown in Table 6. More details of the material characteristics and properties of the HSS sections can be found in Skalomenos and Papazafeiropoulos.[31]

TABLE 6 Material properties of the column HSS section based on coupon test results.

Part	Elastic modulus (GPa)	Yield stress (YS) (MPa)	Ultimate stress (US) (MPa)	Strain at US (%)
Flange	193	346	525	20.5
Corner	172	487	585	5.70

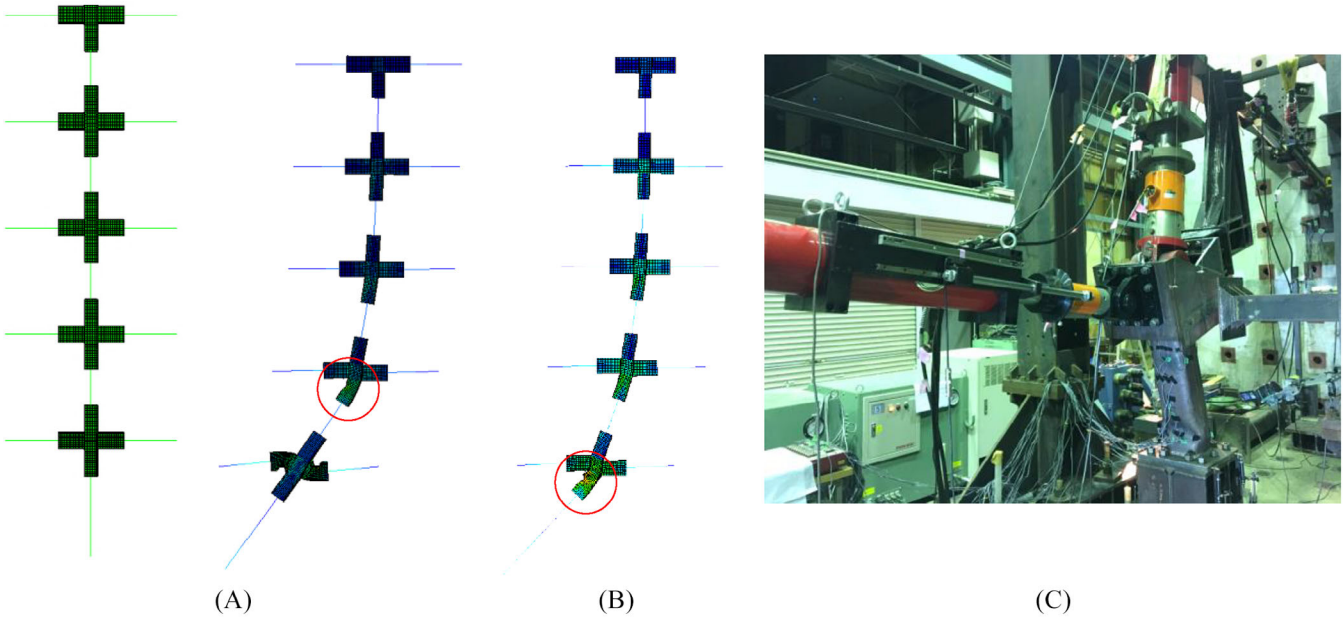

FIGURE 9 Collapse simulation in the proposed hybrid test method (A) SP1 and (B) SP2; (C) overall deformation of the column test at the ultimate loading state.

One additional column was fabricated in order to carry out an isolated column test under the cantilever scheme (fixed bottom end—free top end) (Table 5). In the isolated column test only actuators 1 and 2 were used to impose the lateral deformation and the axial load, respectively. Axial loads remained constant and equal to 25% of the axial column strength.

7 | COLLAPSE HYBRID SIMULATIONS

7.1 | Overall behavior

Figure 9A,B illustrates the FE substructure models for the SP1 and SP2 at the initial and final loading position, respectively. The fishbone model of SP1 deforms in a collapse mechanism that involves the first two storeys, while the fishbone model of SP2 deforms in a collapse mechanism that involves the first storey only (i.e., ground floor). The collapse mechanism of SP1 is identical with the one observed in the FE analysis of the entire building model, as shown in Figure 1A, thus confirming the discussion in Figure 5 for the effectiveness of the adopted fishbone modeling technique to successfully simulate the inelastic behavior of the entire frame. At the ultimate loading state of SP1, plastic hinges were formed at the top end of the second-storey column just below the panel zone and at the beam ends of the first storey (ground floor). The base of the column and beam ends experienced severe local buckling (Figure 9A). At the ultimate loading state of SP2, plastic hinges formed at the top end of the ground-floor column just below the panel zone and at the beam ends of the ground floor. Figure 9C illustrates an overall view of the ultimate deformation of the tested column during the hybrid test. Severe local buckling was observed at the base of the column test. By increasing the height of the ground floor 500 mm in real scale, a different collapse mechanism was observed. The frame with the taller ground floor (SP2) introduced higher rotational demands at the ground-floor columns for a given roof drift compared to the model with the shorter ground floor (SP1), thus resulting in a higher degradation effect and more severe local buckling evolution at the base of the column.

Figure 10A shows the pushover curve for the framed structure as obtained during the hybrid simulations SP1 and SP2. The fundamental natural period T of the frame model was 0.988 s for the SP1 and 1.033 for the SP2, respectively. The

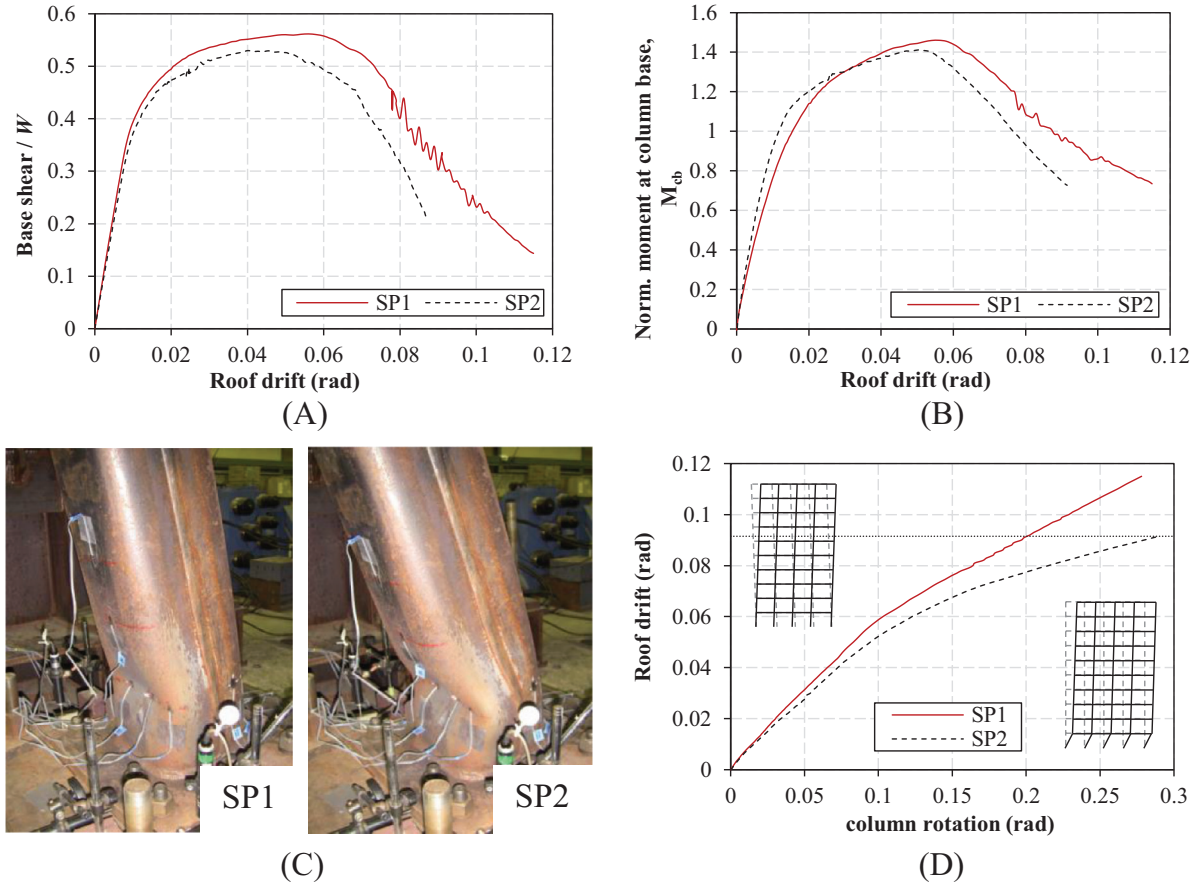

FIGURE 10 Test results as obtained from hybrid testing: (A) normalized base shear against roof drift of the frame; (B) normalized bending moment at the base of the ground floor column test against roof drift of the frame; (C) rotation of the column tests at the 0.0915 roof drift level; (D) roof drift–column test rotation relationship.

pushover curve is presented in the typical fashion: total lateral force on the building (base shear force) normalized by the weight of the fishbone frame model on the vertical axis versus roof drift on the horizontal axis. The weight of the fishbone model W is equal to the total building's weight divided by three (number of the seismic resistant frames) and then divided by five for distributing equally the weight to the six columns. The building is seen to have an over-strength of two relative to its design base shear of 0.26 W.[32] The pushover curve of SP1 reaches 0.56 W at a roof drift of 0.058 radians and then descends, while that of SP2 reaches 0.52 W at a roof drift of 0.048 radians and then descends. The descending branch drops more steeply after reaching a roof drift of 0.07 radians in SP2 than in SP1. Initial stiffness of SP2 is 8.5% lower than in SP1. The concentration of the damage within the ground floor in SP2 led to a smaller global ductility compared to SP1 where a better plastic engagement of the building members was observed in the global deformation mechanism.

Figure 10B plots the bending moment at the base of the column test, M_{cb}, against the roof drift of the frame as obtained by the hybrid simulations. The M_{cb} is normalized by the plastic moment of the square tubular column, M_{cp}. The maximum $M_{cb,max,SP1}$ was 227 kN m and the $M_{cb,max,SP2}$ was 219 kN m (measured experimental values). The calculated M_{cp} of the section is 155.60 kN m using the flange yield stress for the entire steel section (Table 6). One can observe that strength degradation in SP1 initiated at a larger roof drift (0.06 radians) than in SP2 (0.051 radians). This strength degradation is mainly caused by the evolution of local buckling. At the target roof drift of 0.0915, the column of SP2 lost almost 50% of its ultimate flexural strength, while the column of SP1 lost 30% of its ultimate flexural strength, as shown in Figure 10B. The less degrading behavior of SP1 is related to the smaller column rotation demand associated with this roof drift, as shown in Figure 10C. This is due to the more uniform plastic engagement of the upper storeys to the global plastic deformation mechanism of the frame.

Figure 10D plots the relationship between the roof drift and the rotation demands on the column test. The rotation demand at the base of the SP2 column was nearly 0.30 radians when the roof drift reached 0.0915 radians, which is a 1.5 times higher rotation demand than the rotation imposed at the base of the SP1 column (i.e., 0.20 radians). As indicated

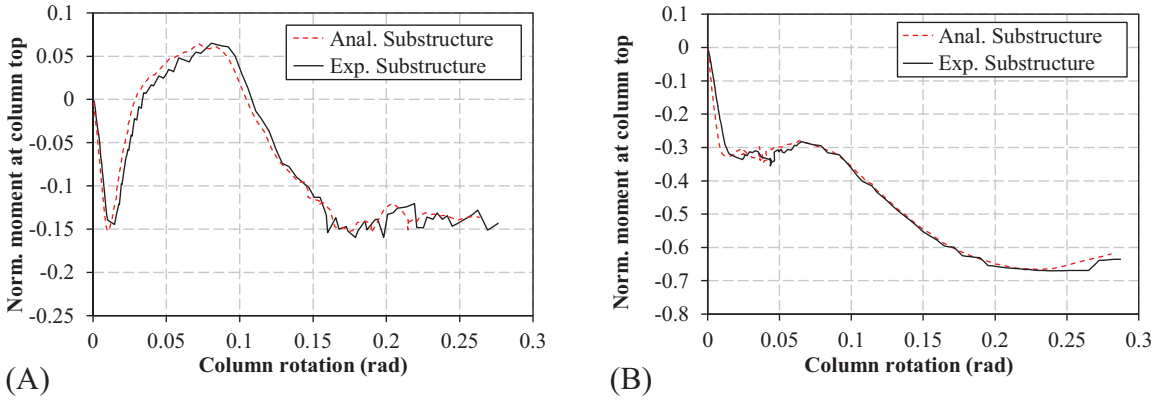

FIGURE 11 Hybrid test consistency: (A) normalized M_{ct}-column rotation relationship in SP1; and (B) normalized M_{ct}-column rotation relationship in SP2.

in Figure 10D, a linear relationship between the frame roof drift and the column test rotation demands indicates the most favorable global plastic deformation mechanism of the structure subject to seismic loads. When concentration of the damage is observed to a particular storey, the gradient of this relationship may significantly reduce. This happened at 6% roof drift in SP1 and at 5% roof drift in SP2 with the latter experiencing steeper change of the gradient between roof drift and column rotation. The proposed test method appears to be effective in correlating global frame response quantities, such as the roof drift and the base shear, with local member responses, such as the ultimate rotational capacity and flexural strength of critical columns. This can enable the direct limitation or control of global response quantities of structures to satisfy performance criteria of critical structural members, thus facilitating rational performance-based design/assessment methods.

7.2 | Loading control and implementation of measured quantities for response prediction

Figure 11 compares the bending moment–rotation relationship between the analytical and experimental column substructure. The bending moment shown in this figure is the one applied at the top end of the column test, M_{ct}, and is normalized by the M_{cp}. Based on these figures one can observe that the proposed hybrid simulation was successful in transferring accurate loads and deformations to the test specimens, as well as in updating the analytical substructure within the force–deformation equilibrium of the whole system. Similar consistency was observed for the bending moment at the base of the ground-floor columns. Thus, the moment distribution along the column test was in good agreement with the FE frame model. The three actuators were synchronized accurately and effectively updated the bending moments and rotations to the column specimen up to the very end of the tests.

In SP1, the experimental rotation of the column at the base was 4.9% higher than the column rotation of the FE model, while in SP2, it was only 3% higher. The error was less than 5% in both tests which proves the rationality of the proposed substructuring techniques (see Section 3). In addition, the variation of the bending moment at the top end of the column test maintains the column curvature (single or double) as it was determined by the FE model. The maximum $M_{ct,max}$ was almost equal to 15% of the M_{cp} for the SP1, and equal to 67% for the SP2. The alteration of the moment distributions along the column length was caused by the stepwise changes of the boundary conditions of the ground-floor column and this was accurately simulated by the proposed online test-set up. More detailed discussion about this is presented in the following section.

As discussed in Section 3.3, a set of experimental values S_i of the column moment M_i and rotation θ_i is used for predicting the spring constant $K_{\theta,i}$ at the base of the FE frame model. The measurement of M_i at the base of the column test is made through the three measured reaction forces at the loading points of the jack and the perpendicular distances of the force vectors taken from the column base (see Figure 8). To calculate the distances of the force vectors, measurements of the displacement transducers were used to calculate the relevant positions of the loading actuators. The implementation of the measured quantities for stiffness prediction highlights the importance of the proposed hybrid simulation in accounting bending moment redistributions not only at high inelastic levels (secant stiffness), but also at the initial stage of the test (initial stiffness). According to the preliminary FE analysis of the entire frame shown in Figure 7B, the bending moment

transferred to the top end of the column test should have remained zero nearly up to a 0.06 roof drift of the frame. Note that the length of the column test is approximately up to the location of the inflection point (i.e., pin location of the column test). However, in hybrid simulations the location of the inflection point in the ground-floor column was found to be different. By implementing the measured stiffness from the column test into the FE frame analysis, the inflection point of the updated model moved at a lower location than the initial location, thus finally subjecting the column test to a double curvature instead of a single curvature. Moreover, by implementing the measured quantities M_i and θ_i the actual material properties of the column, strain hardening effects, and local buckling behavior are directly reflected in the frame analysis. This continuous update of the frame model with measurement quantities strongly affects its inelastic behavior and subsequently, the test demand, and hence the capacity of column test. The following section discusses in detail the structural behavior of the frame model and the column test during the hybrid simulations focusing on the evolution of the overall deformation mechanism of the frame to collapse and the sequence of the individual failures in peripherical members in association with the changes of the boundary conditions to the column test caused by the movement of the inflection point.

7.3 | Bending moment redistribution

Figure 12 presents an overview of the SP1 hybrid simulation. More specifically, Figure 12A schematically defines four damage stages related to the bending moment redistribution along the column length and the location of the inflection point. These damage states are the: (a) Zone I, (b) Zone II, (c) Zone III, and (d) Zone IV. The zones have been highlighted with grey colors in Figure 12B–D where the experimental M_{ct}, the experimental M_{cb}, and the computational bending moment of the beam at the ground floor, M_b, are plotted against the frame roof drift, respectively. Figure 12E depicts the associated deformation and yield areas of the first two storeys of the frame as obtained from the FE analysis.

- Zone I (0–0.01 roof drift) refers to the pre-yielding behavior of the frame. M_{cb} increased linearly until yielding of the ground-floor beams, $M_{b,y}$, as shown in Figure 12C,D, respectively. Under these conditions, M_{ct} proportionally increased taking negative values (Figure 12B), thus subjecting the column test to double curvature.
- Zone II (0.01–0.06 roof drift) refers to the post-yielding behavior of the frame. Ground-floor beams and panel zones yielded nearly at 1% roof drift and entered into the plastic region ($M_{b,p}$) (Figure 12D), while the column test gradually yielded forming a plastic hinge at its base ($M_{cb,p}$) (Figure 12C). The second-storey beams and the panel zones have also yielded, as shown in Figure 12E. The higher rigidity of the base of the ground-floor column compared to the more flexible column top end attracted higher loads and the bending moment at the base of the column increased faster (Figure 12A). The inflection point moved upwards and M_{ct} reached positive values at the end of Zone II (Figure 12B). The column test was subjected to single curvature. At nearly a 2.5% roof drift, the top end of the ground-floor, second-storey, and third-storey column alongside with their corresponding panel zones yielded, as shown in Figure 12E (yielding is denoted by grey color in the stress distribution contour). The fourth-storey beams and panel zone yielded at 3% roof drift. These failure sequences may have caused the gradual change in the bending moment distribution along the column test within Zone II (Figure 12B).
- Zone III (0.06–0.08 roof drift) refers to the post-local buckling behavior of the frame after the onset of local buckling at the base of the column test and at the ends of the ground-floor beams. At 6% roof drift the column test experienced local buckling at its base ($M_{cb,lb}$) and entered the strength degradation phase (Figure 12C). Excessive yielding was observed in the panel zone, column, and beams of the second and third storey (Figure 12E). A bit later, at 7% roof drift, the ground-floor beam exhibited local buckling at its end ($M_{b,lb}$) and entered the strength degradation phase (Figure 12D). The inflection point moved toward the mid-height of the column, as shown in Figure 12A (Zone III). M_{ct} reached negative values at the end of Zone III, and the column test was subjected again to double curvature.
- Zone IV (0.08–0.12 roof drift) refers to the post-local buckling behavior of the frame after the onset of local buckling at the top end of the second-storey column (Figure 12E). Local buckling at the base of the column test and at the ends of the ground-floor beams caused the top end of the second-storey column to buckle at 8% roof drift. Rotation demands at the beam ends were also affected by the gradual formation of the plastic hinge at the top end of the second-storey column (Figure 12E). This led to a severe strength degradation of the beam flexural resistance as the roof drift increased. The bending moment at the bottom end and top end of the ground-floor column reduced at the same rate, thus maintained unchanged the location of the inflection point along the column length.

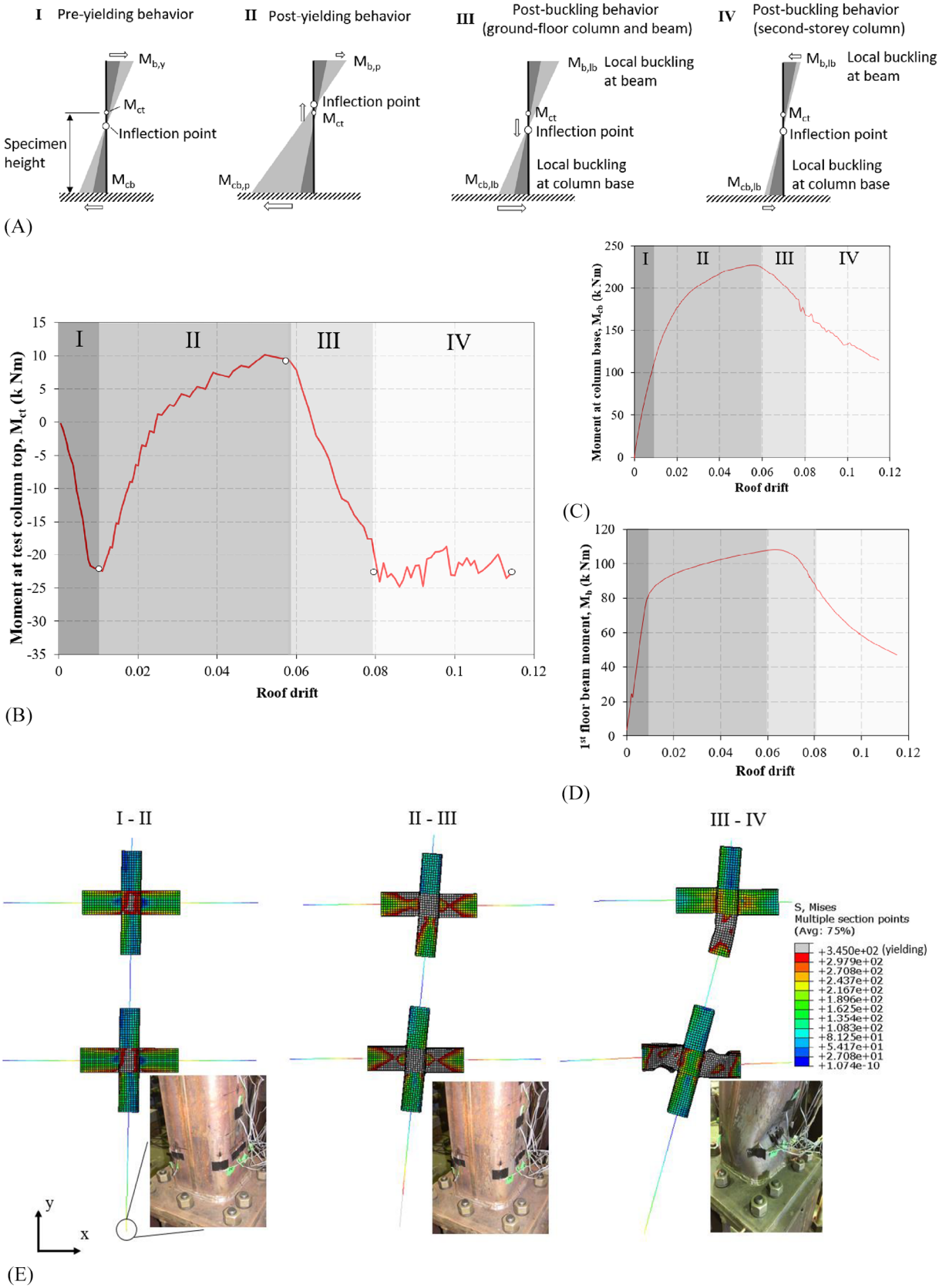

FIGURE 12 Hybrid simulation of SP1: (A) bending moment at the top end of the column test; (B) bending moment at the base of column test; (C) bending moment of ground-floor beam; (D) bending moment distribution at each damage state; (E) frame and column test overall behavior.

Figure 13 presents an overview of the hybrid test results in SP2 in the same manner as in Figure 12. The four zones are as follows:

- Zone I (0–0.01 roof drift) refers to the same damage state as in SP1. M_{cb} increased linearly until yielding of the ground-floor beams, as shown in Figure 13C,D. M_{ct} increased taking negative values (Figure 13B), thus subjecting the column test to double curvature.
- Zone II (0.01–0.05 roof drift) refers to the same damage state as in SP1. Ground-floor beams and panel zones yielded nearly at 1% roof drift and entered the plastic region (Figure 13D). Second-storey beams and panel zones yielded at a slightly higher roof drift than in SP1, nearly at 1.1%, as shown in Figure 13E. The inflection point moved upwards as in SP1 and M_{ct} stopped increasing, as shown in Figure 13A,B. The column test was subjected to double curvature. At 1.6% roof drift, beams of the third storey yielded, while at 2.3% roof drift, the top end of the ground-floor, second-storey, and third-storey column alongside with the corresponding panel zones yielded, as shown in Figure 13E. All these failure sequences seem to affect the bending moment distribution of the ground-floor column in a similar manner as in SP1 (Figure 13B). The fourth-storey beams and panel zones yielded nearly at 3% roof drift. No yielding was observed in the fifth storey.
- Zone III (0.05–0.075 roof drift) refers to a similar damage state as in SP1. Zone III refers to the post-local buckling behavior of the frame after the onset of local buckling at the base of the column test. At 5% roof drift the column test experienced local buckling at its base and entered the strength degradation phase (Figure 13C). Excessive yielding was observed in panel zone, column, and beams of the second storey (Figure 13E). A slight local buckling was observed at the ends of the ground-storey beam nearly at 7% roof drift. The inflection point moved towards the mid-height of the column, as shown in Figure 13A (Zone III). M_{ct} increased significantly taking negative values, as shown in Figure 13B.
- Zone IV (0.075–0.092 roof drift) is different than in SP1. Zone IV in SP2 describes the post-local buckling behavior of the frame after the onset of local buckling at the top end of the ground floor column. Although the top end of the second-storey column indicated a gentle initiation of local buckling, this failure was not fully developed as in SP1. The sudden drop of the flexural strength of the ground-floor beam shown in Figure 13D is related to the local buckling that occurred at the top end of the ground-floor column (Figure 13E). As a result, the evolution of local buckling stopped in the ground-floor beams and the second-storey column. It seems that the taller ground-floor of SP2 than that of SP1 caused a higher overturning moment at this inelastic level and formed a weak-storey mechanism that involved only the ground floor. The bending moment at both ends of the ground-floor column reduced at the same rate, thus no significant change on the location of the inflection point was observed.

7.4 | Axial loads and axial shortening

Figure 14 presents the compressive axial loads and axial shortening of the column test for the SP1 and SP2 hybrid simulation. As it is mentioned in Section 5.2 fishbone boundaries and axial loads are updated during the hybrid simulation. Axial loads vary at similar levels in both specimens, as shown in Figure 14A, remaining almost constant. It is reminded here that the column test is a central column of the frame, as shown in Figure 3A, and no significant influence on the gravity loads is expected by the seismic overturning loads. Figure 14B compares the axial shortening exhibited by SP1 and SP2 during the tests. This figure confirms that the 6% and 5% roof drift can be considered as the critical limit of local buckling initiation in each specimen, respectively. SP1 exhibited a total axial shortening of 19.2 mm at a roof drift of 11.5%, while SP2 exhibited a total axial shortening of 18.8 mm at a roof drift of 9.15%. By comparing the two specimens, SP1 exhibited less severe local buckling and smaller axial shortening due to its better global collapse mechanism. At the roof drift level of 9.15%, SP1 exhibited an axial shortening of 9.3 mm which is almost 50% smaller than that of SP2.

8 | COMPARISON BETWEEN HYBRID SIMULATIONS AND ISOLATED COLUMN TEST

This section compares the hybrid simulation results with the isolated column test (Table 5). Figure 15A illustrates the normalized flexural strength of each column against the column rotation, which is defined as the lateral displacement over the column length. The isolated column exhibited a smaller yielding rotation and 7% lower flexural strength than the columns tested with the proposed hybrid method, while local buckling initiated earlier. Local buckling followed by strength reduction was observed in SP1 and SP2 nearly at 10% storey drift, while in isolated column test local buckling initiation was observed nearly at 7.7% storey drift. As a result, the isolated column experienced more severe axial shortening

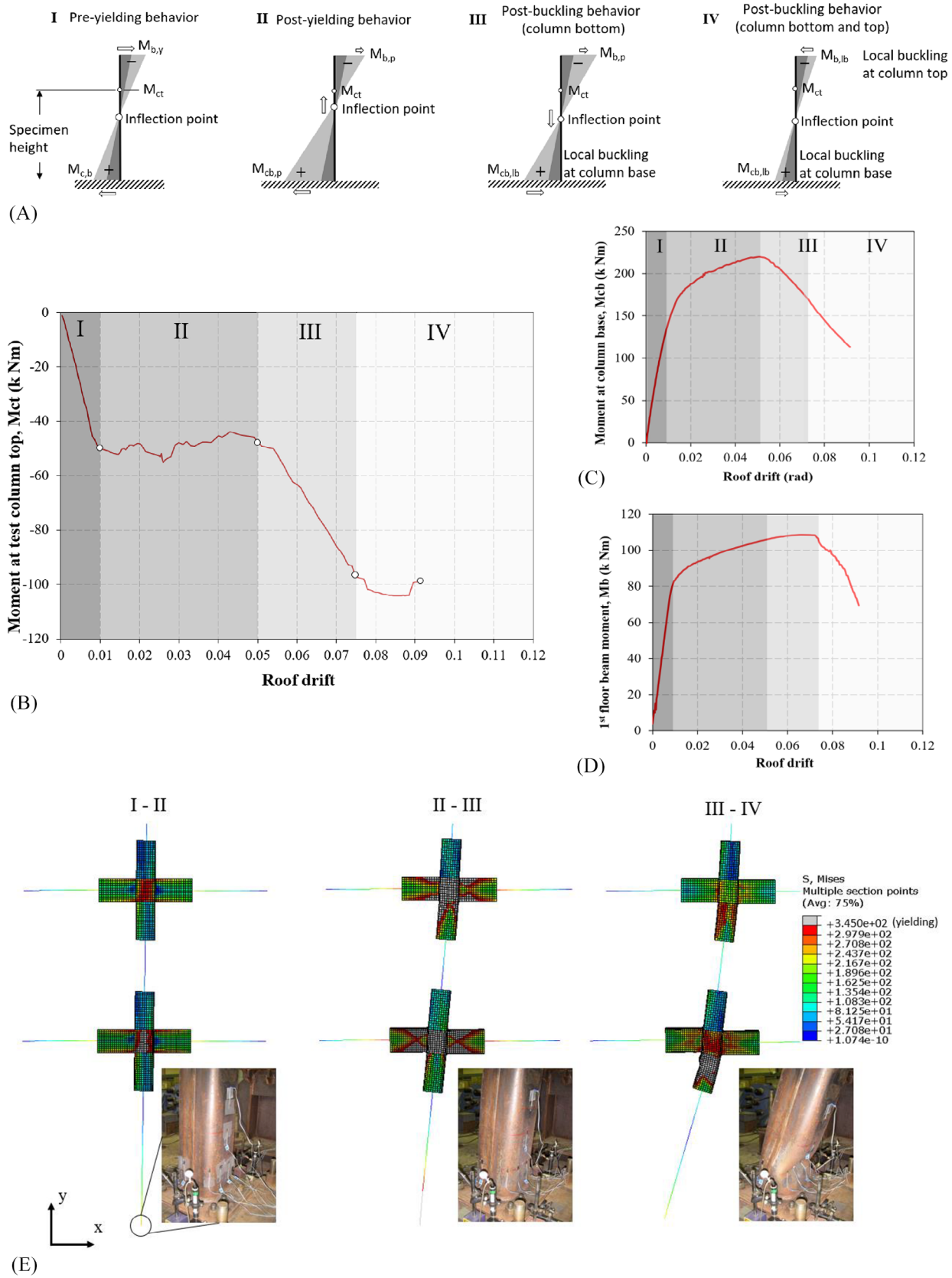

FIGURE 13 Hybrid simulation of SP2: (A) bending moment at the top end of the column test; (B) bending moment at the base of column test; (C) bending moment of ground-floor beam; (D) bending moment distribution at each damage state; (E) frame and column test overall behavior.

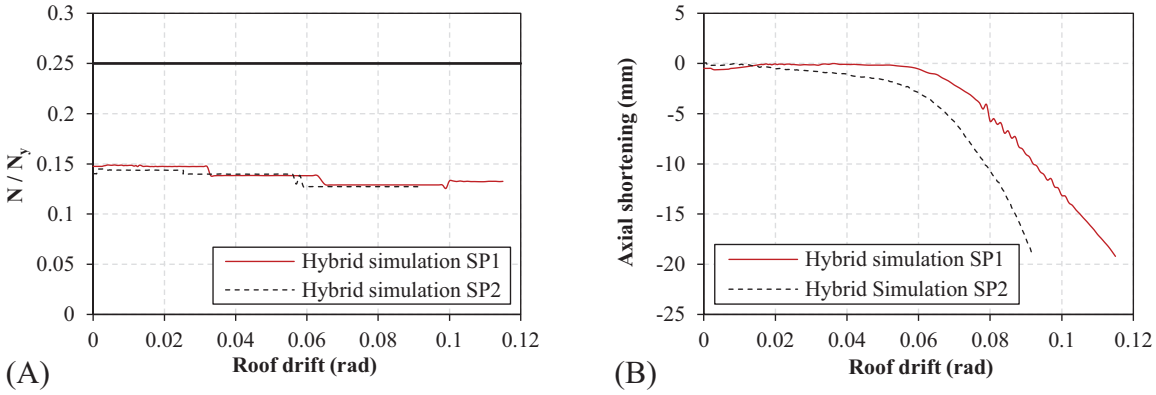

FIGURE 14 Hybrid simulation results for SP1 and SP2: (A) normalized axial load; (B) axial shortening.

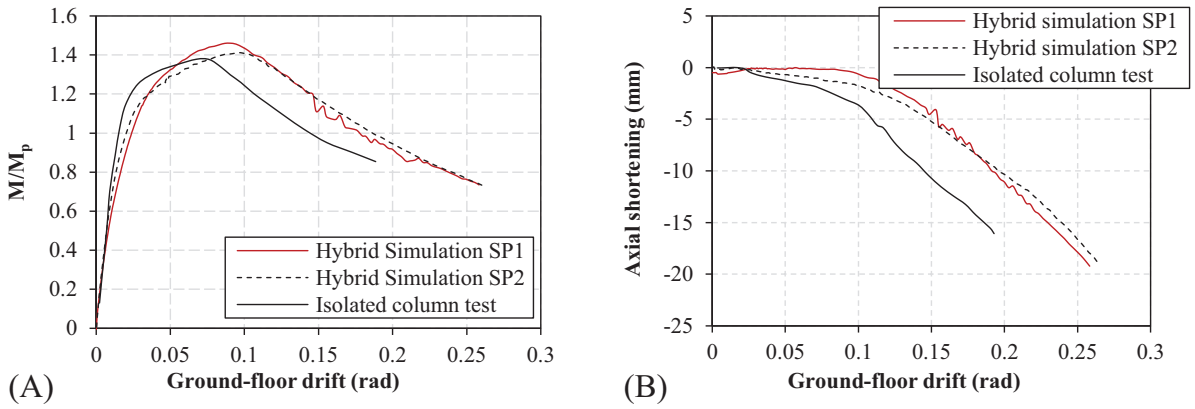

FIGURE 15 Comparison between hybrid simulations and isolated column tests: (A) normalized bending moment at column base versus storey drift; (B) axial shortening versus column rotation.

than the column of SP1 and SP2 (i.e., 1.60 times larger), as indicated in Figure 15B. The more favorable behavior of the columns tested by the proposed hybrid simulation is likely to be related to the consideration of the flexibility of boundary conditions caused by the movement of the inflection point. In addition to this, axial loads in hybrid tests are continuously updated based on the online FE analysis of the frame. Figure 15B also compares the axial load ratio of SP1 and SP2 with that of the isolated column test (i.e., 0.25). The higher axial load ratio in the isolated test has further affected the inelastic behavior of the column. Further studies are required to evaluate the effect of boundary conditions on the behavior of columns and quantify through a systematic investigation its observed favorable impact to critical design quantities of columns, such as yielding rotation, ultimate flexural strength, and ductility.

9 | CONCLUSIONS

A collapse hybrid simulation which uses the nonlinear adaptive static (pushover) analysis to experimentally evaluate the inelastic behavior of ground-floor columns to seismic collapse was presented. The method was validated on two full-scale five-storey five-bay steel moment-resisting frames (MRF) designed according to the Japanese seismic design code. One MRF (SP1) had a ground floor height equal to 4.60 m (i.e., 1.16 times the height of each storey above), while the other MRF (SP2) had a ground floor height equal to 5.10 m (i.e., 1.30 times the height of each storey above). Main conclusions of the present study are as follows:

- The proposed hybrid simulation uses refined finite element modeling methods and fishbone modeling techniques for simulating global collapse. Failures related to strength and stiffness reduction, such as shear inelastic deformation of panel zones and local buckling of beams and columns, are simulated with good accuracy. A novel overlapping boundary

technique and a non-iterative prediction algorithm are integrated to update flexibility of the boundary conditions of the experimental substructure and implement the test information into the analysis procedure including column stiffness, column flexural strength, and column axial shortening.

- Regarding the global plastic deformation mechanism of the tested MRFs, a better plastic engagement of the upper storeys in the short ground-floor MRF was observed (SP1 frame). The SP2 frame with the tall ground floor deformed in a global collapse mechanism that involved mainly the ground floor (weak storey mechanism). The SP1 frame with the short ground floor deformed in a global collapse mechanism that involved both the ground floor and the second storey, thus resulting in lower rotational demands to the ground-floor columns (up to 50% lower).
- The pushover curve of SP1 reached 0.56 W at a roof drift of 0.058 radians and then descended, while that of SP2 reached 0.52 W at a roof drift of 0.048 radians and then descended. The descending branch dropped more steeply in SP2 than in SP1. This strength degradation was mainly caused by the evolution of local buckling at tested column. At the target roof drift of 0.0915, the column test of SP2 lost almost 50% of its ultimate flexural strength, while the column test of SP1 lost 30% of its ultimate flexural strength. Initial stiffness of SP2 was found to be 8.5% lower than in SP1.
- The alteration of moment distribution along the length of the ground-floor column was successfully reproduced in the column test through the proposed hybrid simulation. The method was able to capture all the failure sequences at a frame level that change boundary conditions of the column test at its top end. The main failure sequence is: (a) yielding of the adjacent beams and panel zones at 1% roof drift (Zone II); (b) local buckling at the base of the column test near at 5%−6% roof drift (Zone III); (c) local buckling at the ends of the adjacent storey beams or columns nearly at 8% (Zone IV).
- The imposed moment distribution to the ground-floor column was significantly influenced by local buckling initiated at the base of the ground-floor columns and beams and could cause the top end of the upper-storey columns to buckle. In SP1, local buckling was observed at the top end of the second-storey column at an 8% roof drift.
- In isolated column test, the column exhibited a smaller yielding rotation and nearly lower flexural strength than the ground-floor columns tested with the proposed hybrid method, while local buckling initiated earlier. Local buckling followed by strength reduction was observed in SP1 and SP2 nearly at 10% storey drift, while in isolated column test local buckling initiation was observed nearly at 7.7% storey drift, indicating the more favorable structural behavior of the former. The isolated column test experienced 1.6 times more severe axial shortening than the ground-floor columns of SP1 and SP2.

ACKNOWLEDGMENTS

Part of this work was financially supported by the International New Exploratory Research Grant (2019H-04 / 3604835687) awarded by the Disaster Prevention Research Institute (DPRI) of Kyoto University (PI: Dr K Skalomenos). The authors are also grateful to Nippon Steel Corporation for the provision of column test specimens. The authors are also greatful to Dr Yoshiki Ikeda, Professor of Kyoto University for their valuable comments and support. The first author would like to specially thank Dr Giuseppe Marzano and Mr Shingo Hamauzu, graduates of Kyoto University, as well as the technicians of Structures Lab in DPRI for their valuable assistance in experiments.

DATA AVAILABILITY STATEMENT

The data that support the findings of this study are available from the corresponding author upon reasonable request.

ORCID

Konstantinos Skalomenos https://orcid.org/0000-0002-0734-3992
Masahiro Kurata https://orcid.org/0000-0003-1624-1127

REFERENCES

1. Baša N, Kopitović Vuković N, Ulićević M, Muhadinović M. Effects of internal force redistribution on the limit states of continuous beams with GFRP reinforcement. *Appl Sci*. 2020;10(11):3973.
2. Elkady A, Lignos DG. Full-scale testing of deep wide-flange steel columns under multi axis cyclic loading: loading sequence, boundary effects, and lateral stability bracing force demand. *J Struct Eng*. 2018;144(2):04017189.
3. Wu TU, El-Tawil S, McCormick JP. Highly ductile limits for deep steel columns. *J Struct Eng*. 2018;144(4):04018016.
4. Zhang X, Ricles JM. Experimental evaluation of reduced beam section connections to deep columns. *J Struct Eng*. 2006;132(3):346-357.
5. Chou C-C, Lai Y-C, Xiong H-C, et al. Effect of boundary condition on the cyclic response of I-shaped steel columns: two-story subassemblage versus isolated column tests. *Earthquake Eng Struct Dyn*. 2022;51:3434-3455.

6. Nakashima M. Hybrid simulation: an early history. *Earthquake Engng Struct Dyn*. 2020;49(10):949-962.
7. Takanashi K, Udagawa K, Seki M, Okada T, Tanaka H. Nonlinear earthquake response analysis of structures by a computer actuator online system (part 1: details of the system). *Trans Arch Instit Jpn*. 1975;229:77-83.
8. Mahin SA, Shing PB. Pseudodynamic method for seismic testing. *J Struct Eng*. 1985;111(7):1482-1501.
9. Pan P, Wang T, Nakashima M. *Development of On-line Hybrid Testing: Theory and Application to Structural Engineering*. Elsevier; 2016.
10. Hashemi MJ, Mosqueda G. Innovative substructuring technique for hybrid simulation of multi-story building through collapse. *Earthquake Eng Struct Dyn*. 2014;43(14):2059-2074.
11. Bursi OS, Abbiati G, Cazzador E, Pegon P, Molina FJ. Nonlinear heterogeneous dynamic substructuring and partitioned FETI time integration for the development of low-discrepancy simulation models. *Int J Numer Methods Eng*. 2017;112:1253-1291. doi:10.1002/nme.5556
12. Pan P, Tada M, Nakashima M. Online hybrid test by Internet linkage of distributed test-analysis domains. *Earthquake Eng Struct Dyn*. 2005;34(8):1407-1425.
13. Wang T, McCormick J, Yoshitake N, Pan P, Murata Y, Nakashima M. Collapse simulation of a four-story steel moment frame by a distributed online hybrid test. *Earthquake Eng Struct Dyn*. 2008;37:955-974.
14. Gao X, Castaneda N, Dyke SJ. Real time hybrid simulation: from dynamic system, motion control to experimental error. *Earthquake Eng Struct Dyn*. 2013;42(6):815-832.
15. Calabrese A, Strano S, Terzo M. Real-time hybrid simulations vs shaking table tests: case study of a fibre-reinforced bearings isolated building under seismic loading. *Struct Control Health Monit*. 2015;22:535-556.
16. Wu B, Chen Y, Xu G, Mei Z, Pan T, Zeng C. Hybrid simulation of steel frame structures with sectional model updating. *Earthquake Eng Struct Dyn*. 2016;45(8):1251-1269.
17. Ou G, Yang G, Dyke S, Wu B. Investigation of hybrid simulation with model updating compared to an experimental shake table test. *Front Built Environ*. 2020;6:103.
18. Skalomenos KA, Kurata M, Nakashima M. On-line hybrid test method for evaluating the performance of structural details to failure. *Earthquake Eng Struct Dyn*. 2018;47(3):555-572.
19. Pinto AV, Pegon P, Magonette G, Tsionis G. Pseudo-dynamic testing of bridges using non-linear substructuring. *Earthquake Eng Struct Dyn*. 2004;33(11):1125-1146.
20. Wang T, Nakashima M, Pan P. On-line hybrid test combining with general-purpose finite element software. *Earthquake Eng Struct Dyn*. 2006;35(12):1471-1488.
21. Del Caprio Ramos M, Mosqueda G, Hashemi J. Large-scale hybrid simulation of a steel moment frame building structure through collapse. *J Struct Eng*. 2016;142(1):04015086.
22. Mahmoud HN, Elnashai AS, Spencer BF, Kwon O-S, Bennier D. Hybrid simulation for earthquake response of semirigid partial-strength steel frames. *J Struct Eng*. 2013;139(7):1134-1148.
23. Shao X, Reinhorn AM, Mettupalayam VS. Real-time hybrid simulation using shake tables and dynamic actuators. *J Struct Eng*. 2011;137(7):748-760.
24. Smith M. ABAQUS/Standard User's Manual, Version 6.16. Providence, RI: Dassault Systèmes Simulia Corp; 2016.
25. Skalomenos KA, Nakashima M, Kurata M. Seismic capacity quantification of gusset-plate connections to fracture for ductility-based design. *J Struct Eng*. 2018;144(10):04018195.
26. Krawinkler H. Cyclic loading histories for seismic experimentation on structural components. *Earthquake Spectra*. 1996;12(1):1-12.
27. Fogarty J, El-Tawil S. Collapse resistance of steel columns under combined axial and lateral loading. *J Struct Eng*. 2016;142(1):04015091.
28. Cravero J, Elkady A, Lignos FG. Experimental evaluation and numerical modeling of wide-flange steel columns subjected to constant and variable axial load coupled with lateral drift demands. *J Struct Eng*. 2020;146(3):04019222.
29. MATLAB version: 9.0.1 (R2016a), Natick, Massachusetts: The MathWorks Inc.; 2016.
30. Panyakapo P. Cyclic pushover analysis procedure to estimate seismic demands for buildings. *Eng Struct*. 2014;66:10-23.
31. Skalomenos KA, Papazafeiropoulos G. A computational method for performing nonlinear adaptive pushover analysis of structures through ABAQUS simulation: Proceedings of 7th COMPDYN International Conference on Computational Methods in Structural Dynamics and Earthquake Engineering, 24–26 June 2019, Heraklion, Crete, Greece, doi:10.7712/120119.7199.19194
32. The Building Center of Japan (BCJ). The Building Standard Law of Japan. BCJ; 2016. https://www.bcj.or.jp/publication/detail/17/
33. Hamauzu S, Skalomenos KA, Kurata M, Theofanous M. Local buckling behaviour of high strength steel tubular columns subjected to one-sided cyclic loading and implications in seismic design of steel MRFs. *Soil Dyn Earthquake Eng*. 2022;154:107115.
34. Freeman SA. Review of the development of the capacity spectrum method. *ISET J Earthq Technol*. 2004;41(1):1-13.
35. Chopra AK, Goel RK. A modal pushover analysis procedure for estimating seismic demands for buildings. *Earthquake Eng Struct Dyn*. 2002;31:561-582.
36. Bracci JM, Kunnath SK, Reinhorn AM. Seismic performance and retrofit evaluation of reinforced concrete structures. *J Struct Eng*. 1997;123(1):3-10.
37. Elnashai S. Advanced inelastic static (pushover) analysis for earthquake applications. *Struct Eng Mech*. 2001;12(1):51-69.
38. Hall JF. On the descending branch of the pushover curve for multistory buildings. *Earthquake Eng Struct Dyn*. 2018;47(3):772-783.
39. Waltz RA, Morales JL, Nocedal J, Orban D. An interior algorithm for nonlinear optimization that combines line search and trust region steps. *Mathematical Prog*. 2006;107:391-408.
40. Grimes RG, Lewis LG, Simon HD. A shifted block Lanczos algorithm for solving sparse symmetric generalized eigenproblems. *SIAM J Matrix Anal Appl*. 1994;15(1):228-272.

41. Papazafeiropoulos G, Muñiz-Calvente M, Martínez-Pañeda E. Abaqus2Matlab: a suitable tool for finite element post-processing. *Adv Eng Software*. 2017;105:9-16.
42. Luco N, Mori Y, Funahashi Y, Cornell CA, Nakashima M. Evaluation of predictors of non-linear seismic demands using 'fishbone' models of SMRF buildings. *Earthquake Eng Struct Dyn*. 2003;32:2267-2288.
43. European Committee for Standardisation (CEN). *EN 1993-1-5. Eurocode 3: Design of steel structures—Part 1–5: Plated structural elements*. CEN; 2006.
44. European Committee for Standardisation (CEN). *EN 1998-1. Eurocode 8. Design of structures for earthquake resistance, Part 1: General rules, seismic actions and rules for buildings.* CEN; 2004.

How to cite this article: Skalomenos K, Kurata M. Collapse hybrid simulation for testing steel building columns subject to boundary condition changes. *Earthquake Engng Struct Dyn*. 2024;53:1612–1637. https://doi.org/10.1002/eqe.4083